

Magnetic field driven metal-insulator phase transition in planar systems

E.V. Gorbar*

Universidade Federal de Juiz de Fora, Juiz de Fora 36036-330, Brazil

V. P. Gusynin

*Bogolyubov Institute for Theoretical Physics, 03143, Kiev, Ukraine
and Department of Physics, Nagoya University, Nagoya 464-8602, Japan*

V.A. Miransky*

Department of Applied Mathematics, University of Western Ontario, London, Ontario N6A 5B7, Canada

I. A. Shovkovy*

*School of Physics and Astronomy, University of Minnesota, Minneapolis, MN 55455, USA
(March 12, 2002)*

A theory of the magnetic field driven (semi-)metal-insulator phase transition is developed for planar systems with a low density of carriers and a linear (i.e., relativistic like) dispersion relation for low energy quasiparticles. The general structure of the phase diagram of the theory with respect to the coupling constant, the chemical potential and temperature is derived in two cases, with and without an external magnetic field. The conductivity and resistivity as functions of temperature and magnetic field are studied in detail. An exact relation for the value of the “offset” magnetic field B_c , determining the threshold for the realization of the phase transition at zero temperature, is established. The theory is applied to the description of a recently observed phase transition induced by a magnetic field in highly oriented pyrolytic graphite.

71.30.+h,

I. INTRODUCTION

Although during recent years there has been important progress in understanding non-Fermi liquid dynamics in dimensions $D > 1$, their understanding is still very far from being complete. It is rather clear that non-Fermi liquid behavior yields examples of sophisticated nonperturbative dynamics which should be described by advanced methods of quantum field theory.

It had been recognized rather long ago that relativistic field models can serve as effective theories for the description of long wavelength excitations in condensed matter systems (for a review, see Ref. 1). In particular, they can be applied to a wide class of (quasi-) planar systems. In this case, the corresponding relativistic theories are 2+1 dimensional, i.e., they are formulated in 2+1 dimensional Minkowski space with two space like and one time like coordinates. It is important that amongst these condensed matter systems are such as high- T_c superconductors and carbon-based materials (for a list of papers using relativistic field approach to these systems see Refs. 2–8).

In this paper, we will develop a consistent approach to studying these systems by making use of so called reduced 3+1 dimensional gauge theories.^{9,10} These theories will share the following common feature. Their gauge fields (e.g., the electromagnetic field) responsible for interparticle interaction would be able to propagate in a 3 dimensional bulk, while fermion fields (e.g., describing electron and hole type quasiparticles) would be localized on 2 dimensional planes. The latter will also be referred to as 2 dimensional branes, or just 2-branes. A typical example of a condensed matter system of this type is graphite. It has been known for a long time that fermionic quasiparticles in graphite are nearly 2 dimensional.¹¹ Besides, graphite is a semimetal whose low energy quasiparticles have nearly linear dispersion law (just like massless relativistic particles).^{11,12,5} The Coulomb interaction between quasiparticles is provided by gauge fields which, unlike the quasiparticles themselves, are 3 dimensional in nature.

Recently, the dynamics of reduced QED has been studied in Refs. 9,10. In those papers, purely relativistic theories were considered: in particular the velocities of both massless fermions and photons were equal to the speed of light c . In realistic condensed matter systems, the Fermi velocity of gapless fermions v_F is of course much less than c . This in turn implies that the static Coulomb forces provide the dominant interactions of fermions. This feature makes quite a difference in the analysis.

In this paper we will describe such “realistic” reduced gauge theories with and without an external magnetic field perpendicular to the basal plane. We are particularly interested in a possibility of a spontaneous generation of a gap in the one-quasiparticle spectrum. This might be viewed as a (semi)metal-insulator phase transition. The influence of the magnetic field, as would become clear in a moment, is very powerful in driving (or “catalyzing”) this type of transitions.

The phenomenon of the magnetic catalysis of dynamical symmetry breaking was established as a universal phenomenon in a wide class of 2+1 and 3+1 dimensional relativistic models in Refs. 13,14 (for earlier consideration

of dynamical symmetry breaking in a magnetic field see Refs. 15,16).

The general result states that a constant magnetic field leads to the generation of a fermion dynamical mass (a gap in a one-particle energy spectrum) even at the weakest attractive interaction between fermions. The essence of this effect is the dimensional reduction $D \rightarrow D - 2$ in the dynamics of fermion pairing in a magnetic field. At weak coupling, this dynamics is dominated by the lowest Landau level (LLL) which is essentially $D - 2$ dimensional.^{13,14} The applications of this effect have been considered both in condensed matter physics^{4,7} and cosmology (for reviews see Ref. 17).

The main motivation of the present study was the experimental data reported in Refs. 18–20 and their interpretation (based on the phenomenon of the magnetic catalysis) suggested in Ref. 7. It was observed in those experiments that samples of highly oriented pyrolytic graphite in an external magnetic field show a qualitative change of their resistivity as a function of temperature, that was interpreted as a metal-insulator phase transition. The effect is clearly seen only for a magnetic field perpendicular to the basal plane, suggesting that the orbital motion of quasiparticles is responsible for the change of the conductivity dependence.

The suggestion of Ref. 7 was that this phenomenon can be a manifestation of the magnetic catalysis, when a dynamical gap, connected with a quasiparticle-hole pairing, is generated in a magnetic field. In this paper, we will develop a detailed theory of the magnetic field driven metal-insulator phase transition in planar systems, based on reduced QED. The general structure of the phase diagram of such systems will be described in two cases, with and without an external magnetic field. The behavior of the electric conductivity (resistivity) in these systems will be described in detail. This will allow us to conclude that, in the presence of a magnetic field, the generation of a dynamical gap in planar systems can indeed manifest itself as a metal-insulator phase transition in the behavior of the resistivity $\rho(T, B)$ as a function of the magnetic field and temperature.

It will be also shown that there exist clearly distinguishable signatures of different types of the phase transition. While the resistivity $\rho(T)$ is a smooth function at the critical point $T = T_c$ in the case of a higher order continuous phase transition, there are a discontinuity and a kink in $\rho(T)$ at $T = T_c$ in the cases of the first order and mean field phase transitions, respectively. The conclusion of the present analysis concerning the possibility of the realization of the scenario of the magnetic catalysis in highly oriented pyrolytic graphite is quite positive.

One of the central results of this paper is an explanation of the existence of an “offset” field B_c observed in the experiments.^{18–20} As we will discuss in detail in Sec. VI, the value B_c determines the threshold for the generation of a dynamical gap at *zero* temperature: it happens only if $B > B_c$. It is remarkable that, as will be shown in Sec. IV, the existence of B_c is a robust consequence of

the mechanism of the magnetic catalysis. Moreover, the *exact* relation for B_c will be pointed out. It is:

$$|eB_c| = \frac{2\pi cn}{N_f}, \quad (1)$$

where N_f is the number of fermion species (“flavors”) and n is a charge density of carriers ($N_f = 2$ in graphite). While the existence of this exact relation is noticeable in itself, its experimental verification would be a critical check of the validity of the magnetic catalysis scenario in highly oriented pyrolytic graphite.

The paper is organized as follows. In Sec. II general features of the model (reduced QED) are described. In Sec. III we analyze the gap equation and establish the phase diagram in reduced QED without magnetic field. In Sec. IV the gap equation in reduced QED with an external magnetic field is studied. The resistivity and conductivity in this system are studied in detail in Sec. V. Sec. VI is devoted to the interpretation of the experimental data in highly oriented pyrolytic graphite. In Sec. VII, we summarize the results of this work. There are also three Appendices. The symmetry of 2+1 dimensional fermions is considered in Appendix A. A derivation of the polarization function and the gap equation in reduced QED is done in Appendix B. In Appendix C, the effective potential for reduced QED with a nonzero chemical potential is derived.

II. MODEL

In this section, we describe the general features of the model. As was mentioned in Introduction, the main assumption of the reduced dynamics of the planar systems is that the fermionic quasiparticles are confined to a flat 2-brane, while the gauge fields are free to propagate in the 3 dimensional bulk.

A similar setting was recently studied in a class of relativistic models in Refs. 9,10. Here, however, we consider a strongly nonrelativistic model (with the Fermi velocity v_F being much less than the speed of light) which could be applied to realistic planar condensed matter systems such as highly oriented pyrolytic graphite, see Fig. 1.

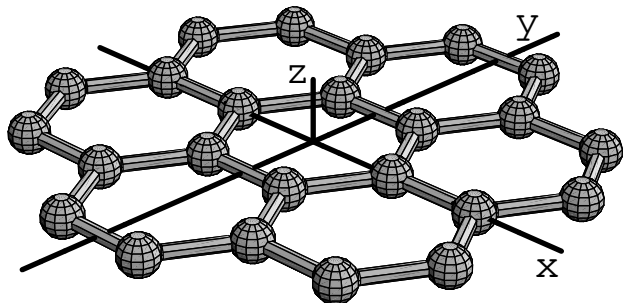


FIG. 1. The schematic lattice structure of a single layer of graphite.

The spatial coordinates on the brane (e.g., a single layer of graphite) are denoted by $\vec{r} = (x, y)$. The orthogonal direction is labeled by the z coordinate. Thus, the most general bulk spatial vector is given by $\vec{R} = (x, y, z)$.

The lagrangian density of the electromagnetic field (in the bulk) is given by

$$\mathcal{L}_{em} = \frac{1}{8\pi} \left(\varepsilon_0 \vec{E}^2 - \frac{1}{\mu_0} \vec{B}^2 \right) - A_0 \rho + \frac{1}{c} \vec{A} \cdot \vec{j}, \quad (2)$$

where ε_0 is the dielectric constant, μ_0 is the magnetic permeability, A_0 and \vec{A} are the scalar and vector potentials. The electric and magnetic fields are

$$\vec{E} = -\vec{\nabla} A_0 - \frac{1}{c} \partial_t \vec{A}, \quad (3)$$

$$\vec{B} = \vec{\nabla} \times \vec{A}. \quad (4)$$

The interacting terms, with the quasiparticle charge density ρ and current \vec{j} , were also included in the lagrangian density in Eq. (2). Now, the lagrangian density of quasiparticles themselves (defined only on the 2-brane) reads

$$\mathcal{L}_0 = v_F \bar{\Psi}(t, \vec{r}) \left(\frac{i\gamma^0(\partial_t + i\mu)}{v_F} - i\gamma^1 \partial_x - i\gamma^2 \partial_y \right) \Psi(t, \vec{r}), \quad (5)$$

where $\Psi(t, \vec{r})$ is a 4-component spinor, $\bar{\Psi} = \Psi^\dagger \gamma^0$, and the 4×4 Dirac γ -matrices furnish a reducible representation of the Clifford (Dirac) algebra in $2+1$ dimensions (see Appendix A).^{21,22} In order to describe the situation with a finite ‘‘residual’’ density of carriers, here the chemical potential μ , connected with the electric charge, was introduced.

We will consider the case when the fermion fields carry an additional, ‘‘flavor’’, index $i = 1, 2, \dots, N_f$ (in the example of graphite, $N_f = 2$, see Refs. 6,7). Then, the symmetry of the lagrangian (5) is $U(2N_f)$ (see Appendix A).

In the case of minimal coupling of the electromagnetic field, the quasiparticle charge density and current take the following explicit form:

$$\rho(t, \vec{R}) = e \bar{\Psi}(t, \vec{r}) \gamma^0 \Psi(t, \vec{r}) \delta(z), \quad (6)$$

$$j_x(t, \vec{R}) = e v_F \bar{\Psi}(t, \vec{r}) \gamma^1 \Psi(t, \vec{r}) \delta(z), \quad (7)$$

$$j_y(t, \vec{R}) = e v_F \bar{\Psi}(t, \vec{r}) \gamma^2 \Psi(t, \vec{r}) \delta(z), \quad (8)$$

$$j_z(t, \vec{R}) = 0. \quad (9)$$

Proceeding as in Ref. 9, the initial action can be reduced to the brane layer. Then, neglecting relativistic corrections of order $(v_F/c)^2$, we are left with the following brane action of interacting quasiparticles:

$$\begin{aligned} S_{qp} \simeq & \int dt d^2 \vec{r} \mathcal{L}_0(t, \vec{r}) - \frac{1}{2} \int dt \int dt' \int d^2 \vec{r} \int d^2 \vec{r}' \\ & \times \bar{\Psi}(t, \vec{r}) \gamma^0 \Psi(t, \vec{r}) U(t-t', |\vec{r}-\vec{r}'|) \\ & \times \bar{\Psi}(t', \vec{r}') \gamma^0 \Psi(t', \vec{r}'), \end{aligned} \quad (10)$$

The exact potential $U(t, |\vec{r}|)$ contains the initial Coulomb interaction as well as the polarization effects on top of it. When the polarization effects of the brane quasiparticles are neglected, the potential takes the following simple form:

$$U_0(t, |\vec{r}|) = \frac{e^2 \delta(t)}{\varepsilon_0} \int \frac{d^2 \vec{k}}{(2\pi)^2} \exp(i\vec{k} \cdot \vec{r}) \frac{2\pi}{|\vec{k}|} = \frac{e^2 \delta(t)}{\varepsilon_0 |\vec{r}|}. \quad (11)$$

Note, however, that in many cases of interest (e.g., in the case of a finite temperature and/or a finite density and/or a nonzero magnetic field), the polarization effects may considerably modify this bare Coulomb potential. Thus, the interaction should rather be given by

$$U(t, |\vec{r}|) = \frac{e^2}{\varepsilon_0} \int \frac{d\omega}{2\pi} \int \frac{d^2 \vec{k}}{2\pi} \frac{\exp(-i\omega t + i\vec{k} \cdot \vec{r})}{|\vec{k}| + \Pi(\omega, |\vec{k}|)}, \quad (12)$$

where the polarization function $\Pi(\omega, |\vec{k}|)$ is proportional (with a factor of $2\pi/\varepsilon_0$) to the time component of the photon polarization tensor.

Adding a mass (gap) term $\Delta_0 \bar{\psi} \psi$ into the action (10) would reduce the $U(2N_f)$ symmetry down to the $U(N_f) \times U(N_f)$ (see Appendix A). Therefore the dynamical generation of a fermion gap (connected with a quasiparticle-hole pairing) will lead to the spontaneous breakdown of the $U(2N_f)$ down to the $U(N_f) \times U(N_f)$.²³ Our goal is the description of the flavor phase transition connected with generating the gap. We will consider the dynamics both with and without an external magnetic field.

III. GAP EQUATION. ZERO MAGNETIC FIELD

In this section we will describe the dynamics of the generation of a gap connected with a quasiparticle-hole pairing provided by the interaction (12) in the case of the zero external magnetic field. We will begin by calculating the polarization function $\Pi(\omega, |\vec{k}|)$. Actually, we will calculate (and use in the gap equation) $\Pi(0, |\vec{k}|)$, i.e., the polarization function in instantaneous approximation. The reliability of this approximation will be discussed in Sec. III E.

A. Polarization function

The one-loop polarization function at finite temperature and finite chemical potential is given by the following integral representation (see Appendix B):

$$\begin{aligned} \Pi(0, \vec{k}) = & \frac{2T e^2 N_f}{\varepsilon_0 v_F^2} \int_0^1 dx \left[\ln \left(2 \cosh \frac{R_x + \mu}{T} \right) \right. \\ & \left. - \frac{\Delta_T^2(\mu)}{2T R_x} \tanh \frac{R_x + \mu}{2T} + (\mu \rightarrow -\mu) \right], \end{aligned} \quad (13)$$

where $R_x = \sqrt{v_F^2 \vec{k}^2 (1-x) + \Delta_T^2(\mu)}$, $\Delta_T(\mu)$ is the fermion gap, and T is temperature. Notice that the gap is a dynamical quantity, determined from a gap equation (see Sec. III B below), and therefore it can depend on both temperature and chemical potential. The retardation effects are neglected here, meaning that the instantaneous exchange approximation is used for the electromagnetic interactions. Since the Fermi velocity v_F is much less than the speed of light c , this approximation should be reliable. Notice that throughout this paper we work in the vacuum in which the fermion gap is positive.

At $\mu = 0$ (zero density) and $T = 0$, the polarization function becomes

$$\Pi(0, \vec{k}) = \frac{e^2 N_f}{\varepsilon_0 v_F^2} \left(\Delta_0 + \frac{v_F^2 \vec{k}^2 - 4\Delta_0^2}{2v_F |\vec{k}|} \arctan \frac{v_F |\vec{k}|}{2\Delta_0} \right). \quad (14)$$

At nonzero density and $T = 0$, the function in Eq. (13) reduces to

$$\Pi(0, \vec{k}) = \frac{2e^2 N_f}{\varepsilon_0 v_F^2} |\mu|, \text{ for } |\vec{k}| \leq k_*, \quad (15)$$

$$\begin{aligned} \Pi(0, \vec{k}) = \frac{2e^2 N_f}{\varepsilon_0 v_F^2} |\mu| & \left[1 - \frac{\sqrt{\vec{k}^2 - k_*^2}}{2|\vec{k}|} + \frac{v_F^2 \vec{k}^2 - 4\Delta_0^2(\mu)}{4\mu v_F |\vec{k}|} \right. \\ & \left. \times \arctan \frac{v_F \sqrt{\vec{k}^2 - k_*^2}}{2\mu} \right], \text{ for } |\vec{k}| > k_*, \quad (16) \end{aligned}$$

where $k_* \equiv 2\sqrt{\mu^2 - \Delta_0^2(\mu)}/v_F$ is proportional to the square root of quasiparticle density at $T = 0$, see Eq. (85) below. As is easy to check, this polarization function has a very strong dependence on momentum. Indeed, while $\Pi(0, \vec{k})$ remains constant for small momenta, $|\vec{k}| \leq k_*$, its value drops considerably for $|\vec{k}| \gtrsim k_*$. In the case of a small density of carriers, i.e., $n \sim k_*^2 \ll (\Delta_0/v_F)^2$, this momentum dependence is particularly strong.

As is clear from Eq. (15), the value of the Debye mass, $M_D \equiv \Pi(0, 0)$, could be quite large in the case of a nonzero gap and small density of carriers. At the same time, the function $\Pi(0, \vec{k})$ at intermediate values of the momenta, $|\vec{k}| \sim \sqrt{k_* \Delta_0(\mu)}/v_F$, is about a factor of $\Delta_0(\mu)/\sqrt{\mu^2 - \Delta_0^2(\mu)}$ smaller, i.e., $\Pi(0, \vec{k}) \sim M_D \sqrt{\mu^2 - \Delta_0^2(\mu)}/\Delta_0(\mu)$. Finally, for $|\vec{k}| \gg \Delta_0(\mu)/v_F$, the polarization tensor approaches the following asymptote:

$$\Pi(0, \vec{k}) \simeq \frac{\pi e^2 N_f}{4\varepsilon_0 v_F} |\vec{k}|. \quad (17)$$

This observation is quite important for the proper analysis of the pairing dynamics between electron and hole types of quasiparticles leading to a possible dynamical generation of a gap. As we shall see below, it is in fact the region of momenta $|\vec{k}| \gg \Delta_0(\mu)/v_F$ that dominates in such a dynamics. This in particular implies that the

one-loop approximation with free gapless fermions (when both the gap and the wave function renormalization are neglected) is a reliable approximation for the polarization function in the gap equation, at least for large N_f . It could work reasonably well even for minor values of N_f of order 1, say, 2 as in graphite.²⁴

B. Dynamical gap at $T = 0$ and $\mu = 0$

Now, let us study a possibility of spontaneous generation of a dynamical gap in the one-particle spectrum of quasiparticles. We begin by considering the gap equation for the zero density case. Its explicit form reads [see Eq. (B8) in Appendix B]

$$\Delta_p = \lambda \int \frac{dq d\mathbf{q} \Delta_q \mathcal{K}(p, q)}{\sqrt{q^2 + (\Delta_q/v_F)^2}}, \quad (18)$$

where the approximate expression for the kernel $\mathcal{K}(p, q)$ is given by

$$\mathcal{K}(p, q) = \frac{\theta(p-q)}{p} + \frac{\theta(q-p)}{q}, \quad (19)$$

and

$$\lambda = \frac{e^2}{2(\varepsilon_0 v_F + \pi e^2 N_f/4)}. \quad (20)$$

It is well known,^{22,25,9} that the approximation with the one-loop polarization function in the kernel of the gap equation (the so called improved rainbow approximation) is reliable for large values of the number of fermion flavors N_f . Here, however, we will also consider the values of N_f of order 1, say, 2 as in graphite. It is reasonable to assume that this approximation works qualitatively (although apparently not always quantitatively) even for these values of N_f , providing a general insight into the nonperturbative dynamics of spontaneous generation of a gap. The analysis done in 2 + 1 dimensional QED supports this assumption.²⁶

In the most important region of momenta $|\vec{k}| \gg \Delta_0/v_F$ where the pairing dynamics dominates (see below), the only role of the term $(\Delta_q/v_F)^2$ in the denominator of the integrand on the right hand side of Eq. (18) is to provide a cutoff in the infrared region. Therefore one can drop this term, introducing instead the explicit infrared cutoff Δ_0/v_F in the integral. This is the essence of the so called bifurcation approximation. As a result, we arrive at the following equation:

$$\Delta_p = \lambda \left(\int_{\Delta_0/v_F}^p \frac{dq}{p} \Delta_q + \int_p^\Lambda \frac{dq}{q} \Delta_q \right). \quad (21)$$

Here we also introduced a finite ultraviolet cutoff Λ . In a condensed matter system, it could be taken of order π/a where a is a characteristic lattice size (for example,

$a = 2.46\text{\AA}$ for graphite). An alternative, equally good, estimate of Λ is as the width of the energy band. In the example of graphite, it is equal to 2.4 eV.

The last integral equation is equivalent to the differential equation,

$$p^2 \Delta_p'' + 2p \Delta_p' + \lambda \Delta_p = 0, \quad (22)$$

with the boundary conditions:

$$p^2 \Delta_p' \Big|_{p=\Delta_0/v_F} = 0, \quad (23)$$

$$(p \Delta_p' + \Delta_p) \Big|_{p=\Lambda} = 0. \quad (24)$$

The solution compatible with the infrared boundary condition (23) reads

$$\Delta_p = \frac{\Delta_0^{3/2}}{\sin(\delta) \sqrt{pv_F}} \sin \left(\frac{\sqrt{4\lambda-1}}{2} \ln \frac{pv_F}{\Delta_0} + \delta \right), \quad (25)$$

where $\delta = \arctan \sqrt{4\lambda-1}$. Notice that Δ_0 satisfies the relation $\Delta_0 = \Delta_{p=\Delta_0/v_F}$. The ultraviolet boundary condition (24) imposes another restriction,

$$\frac{\sqrt{4\lambda-1}}{2} \ln \frac{v_F \Lambda}{\Delta_0} + 2\delta = \pi. \quad (26)$$

As is clear from this equation, a meaningful solution for the dynamical gap, satisfying the constraint $\Delta_0 \ll \Lambda v_F$, exists only for $\lambda > 1/4$. In the nearcritical region, i.e., when $\sqrt{4\lambda-1}$ is small, the gap reads

$$\Delta_0 \simeq \Lambda v_F \exp \left(-\frac{2\pi}{\sqrt{4\lambda-1}} + 4 \right). \quad (27)$$

The condition $\lambda > 1/4$ gives the critical line in the plane (g, N_f) , where the dimensionless coupling constant is $g \equiv e^2/\varepsilon_0 v_F$:

$$g_{cr} = \frac{4}{8 - \pi N_f}, \quad (28)$$

which means that, in absence of an external magnetic field, a dynamical gap is generated only if $g > g_{cr}$. In the example of graphite, the number of ‘‘flavors’’ is equal 2. Thus, the estimate of its critical coupling gives $g_{cr} \approx 2.33$. We emphasize that it is just an estimate obtained in the leading order in $1/N_f$ in instantaneous approximation. For $N_f = 2$ as in graphite, both $1/N_f$ corrections and improving the instantaneous approximation can certainly vary this value (see a discussion in the end of Sec. III E).

If highly oriented pyrolytic graphite is a semimetal in absence of an external magnetic field, it is clear that its effective coupling g_{eff} (defined, for example, at the energy scale below which the Dirac type effective action provides an appropriate description of the quasiparticle dynamics) is smaller than g_{cr} . Indeed, if the interaction were stronger than this, the ground state rearrangement

(from a semimetal to an insulator state), caused by the particle-hole pairing, could not be prevented.

Let us now discuss the self-consistency of our assumption that the region of momenta $|\vec{k}| \gg \Delta_0/v_F$ is mostly responsible for the generation of a ‘‘small’’ gap $\Delta_0 \ll \Lambda v_F$ in the nearcritical limit. The point is that in this regime the logarithm $\ln(\Lambda v_F/\Delta_0) \sim 2\pi/\sqrt{4\lambda-1}$ is large. On the other hand, the behavior of the integrand on the right hand side of Eq. (18) is smooth as $q \rightarrow 0$. The smooth behavior of the integrand in the infrared region implies that the region $0 \leq q \lesssim \Delta_0/v_F$ is too small to generate the large logarithm $\ln(\Lambda v_F/\Delta_0)$. This logarithm [and therefore the essential singularity in expression (27)] is generated in the large region $\Delta_0/v_F \ll q \ll \Lambda$. A variation of the kernel in the infrared region can at most change the overall coefficient in the expression for the gap.

At this point, we would like to mention that the dimensionless coupling constant in the problem at hand is $g \equiv e^2/\varepsilon_0 v_F$. In the gap equation, g has to be considered as the bare coupling constant and its value can be large. As was shown in Ref. 6, in the absence of a dynamical gap, the corresponding renormalization group (running) coupling runs logarithmically to a trivial fixed point in infrared. In the presence of the gap, such running should stop at the energy scale of order Δ_0 . This means that the nonperturbative dynamics shifts the zero infrared fixed point to a finite value.

C. Dynamical gap at $T \neq 0$ or $\mu \neq 0$

Up to now, we have considered the case with the zero density and zero temperature. It is clear that the critical value of the coupling constant should be larger than $g_{cr} \approx 2.33$ if a nonzero density (and/or finite temperature) are taken into account. Indeed, with increasing the charge density of carriers or the value of the temperature, the screening effects get stronger and the quasiparticle interactions get weaker. Besides that, the pairing between quasiparticles in the two adjacent bands separated by the dynamical gap gradually becomes less efficient. The latter could be clearly seen by comparing the energy gain from creating a gap in the spectrum and the energy loss of pushing up the energy of all the states in the band above the gap. Both effects work against the formation of a gap. Thus, after reaching some critical value, the finite density or temperature effects will be so strong that dynamical generation of a gap will be impossible.

When the chemical potential is smaller than the gap, the dynamics of the zero temperature model remains unchanged. Thus for all values of $\mu < \Delta_0 \equiv \Delta_0(\mu)|_{\mu=0}$, the exact solution for the dynamical gap is the same. In our approximation, it is given by Eq. (27). In order to consider the possibility of a nontrivial solution satisfying the condition $\mu > \Delta_0(\mu)$, we consider an approximate gap equation following from Eq. (17) and Eqs. (B8), (B9)

taken in the limit $T \rightarrow 0$:

$$\Delta_p = \lambda \left(\int_{\epsilon}^p \frac{dq}{p} \Delta_q + \int_p^{\Lambda} \frac{dq}{q} \Delta_q \right), \quad (29)$$

where the infrared cutoff ϵ is given by a larger value of $\Delta_0(\mu)/v_F$ or $\sqrt{\mu^2 - \Delta_0^2(\mu)}/v_F$. By making use of the same method as before, we straightforwardly derive two branches of the solution:

$$\Delta_0(\mu) \simeq \Delta_0, \quad (30)$$

for $\mu < \sqrt{2}\Delta_0$ (here we took into account that $\Delta_0(\mu) = \Delta_0$ for $\mu < \Delta_0$), and

$$\Delta_0(\mu) \simeq \sqrt{\mu^2 - \Delta_0^2}, \quad (31)$$

valid for $\Delta_0 \leq |\mu| \leq \sqrt{2}\Delta_0$. While the first branch of the solution in Eq. (30) describes a gap that is essentially unchanged with μ , the value of the gap along the second branch of the solution in Eq. (31) increases with the chemical potential. For the values of the chemical potential in the range $\Delta_0 \leq \mu \leq \sqrt{2}\Delta_0$, both branches of the solution coexist. The first branch corresponds to a locally stable solution (i.e., to a local minimum of the effective potential), while the other one — to an unstable solution (i.e., to a local maximum of the effective potential). In addition, there is always a trivial solution which corresponds to an extremum of the effective potential at the origin. When both nontrivial solutions (30) and (31) coexist, the extremum at the origin should be a minimum. This follows from a simple consideration of the topology of the effective potential.

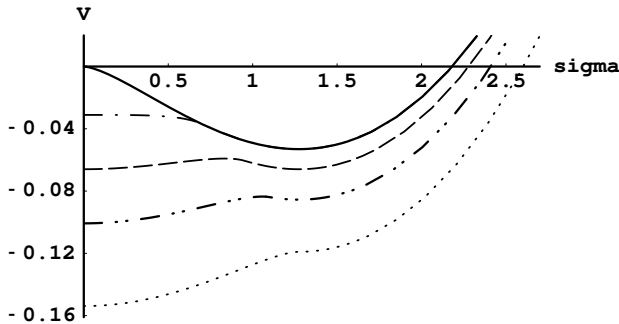


FIG. 2. The effective potential of the composite field σ for a few different values of the chemical potential: $\mu = 0$ (solid line), $\mu = \Delta_0$ (dash-dotted line), $\mu = \mu_c \approx 1.19\Delta_0$ (dashed line), $\mu = 1.3\Delta_0$ (dash-dot-dotted line), and $\mu = \sqrt{2}\Delta_0$ (dotted line). In calculation, we used $\Delta_0 = 1$. The values of the potential are given in units of $N_f \Delta_0^3 / v_F^2$, and values of the composite field σ — in units of $N_f (\Delta_0 / v_F)^{3/2} \sqrt{\Lambda}$.

Of course, the analysis of the gap equation alone would not be sufficient to prove most of the above statements. To support them, we derived the effective potential $V(\sigma)$ as a function of the composite field $\sigma = -\langle \bar{\psi}\psi \rangle$ in Appendix C. This potential is graphically shown in Fig. 2

for a few different values of the chemical potential. As is clear from the figure, we have a typical realization of the first order phase transition.

Our analysis of the effective potential also allows to determine the critical value of the chemical potential:

$$\begin{aligned} \mu_c &\simeq \frac{\Delta_0}{(2 - \sqrt{2})^{1/3}} \\ &\simeq \frac{\Lambda v_F}{(2 - \sqrt{2})^{1/3}} \exp\left(-\frac{2\pi}{\sqrt{4\lambda - 1}} + 4\right). \end{aligned} \quad (32)$$

When the chemical potential increases from $\mu = \mu_c - 0$ to $\mu = \mu_c + 0$, the value of the gap drops from $\Delta \simeq \Delta_0$ down to $\Delta = 0$.

Similarly, at $\mu = 0$, we could derive the value of the critical temperature. It also appears to be of the same order as Δ_0 :

$$T_c \simeq \frac{\Delta_0}{2} \simeq \frac{\Lambda v_F}{2} \exp\left(-\frac{2\pi}{\sqrt{4\lambda - 1}} + 4\right). \quad (33)$$

Unlike the case with the chemical potential, the phase transition in temperature is of the second order. This follows both from the existence of a single-branch solution to the gap equation and from a direct study of the effective potential.

D. Reduced QED₃₊₁ vs. conventional QED₂₊₁

Before concluding this section, it is instructive to compare the reduced dynamics in the 2-brane model at hand with the “conventional” QED₂₊₁. The gap equations in these two models are similar, but the interaction potentials are slightly different. Instead of expression (12), one has^{22,25}

$$U_{3d}(t, \vec{r}) = \frac{e_3^2}{\varepsilon_0} \int \frac{d\omega}{2\pi} \int \frac{d^2 \vec{k}}{(2\pi)^2} \frac{\exp(-i\omega t + i\vec{k} \cdot \vec{r})}{\vec{k}^2 + \Pi(\omega, |\vec{k}|)}, \quad (34)$$

where e_3 is the (dimensionful) coupling constant in QED₂₊₁ and, in the relevant region of momenta $\Delta \ll v_F |\vec{k}| \ll e_3^2 / \varepsilon_0 v_F$, the polarization function here is essentially the same as in Eq. (13), except that the dimensionless coupling constant $e^2 / \varepsilon_0 v_F$ is replaced by the dimensionful $e_3^2 / \varepsilon_0 v_F$. Comparing expressions (34) and (12), one can see that the only difference between them is in the appearance of the term \vec{k}^2 , instead of $|\vec{k}|$, in the denominator of the former. This point makes quite a difference. On the one hand, it provides a dynamical ultraviolet cutoff $\sim e_3^2$ in the SD equation and, on the other hand, since this term is suppressed in the region $v_F |\vec{k}| \ll e_3^2 / \varepsilon_0 v_F$, it is irrelevant for generating the gap. This implies reducing screening of Coulomb like interactions in QED₂₊₁ as compared to the reduced dynamics. Let us consider this point in more detail. It is easy to find that the dynamical gap in QED₂₊₁ is

$$\Delta_{3d} \simeq \frac{e_3^2}{\varepsilon_0 v_F} \exp\left(-\frac{2\pi}{\sqrt{4\lambda_3 - 1}} + 4\right), \quad (35)$$

where $\lambda_3 = 2/\pi N_f$. Since this solution exists when $\lambda_3 > 1/4$, it implies that the critical value of N_f is equal to $8/\pi \approx 2.55$. The same critical value for N_f was obtained in Ref. 8.

Now, notice that the parameter λ_3 coincides with λ in Eq. (20) only in the limit $e^2 \rightarrow \infty$. Thus, the reduced dynamics becomes equivalent to QED₂₊₁ dynamics only in the maximally strong coupling limit, with $e^2 \rightarrow \infty$. Therefore, we conclude that there are important similarities and important differences between the dynamics in QED₂₊₁ and reduced QED₃₊₁ with a 2-brane. Both dynamics are intimately connected with long range Coulomb like interactions. On the other hand, since QED₂₊₁ is superrenormalizable (and therefore asymptotically free) theory, its nonperturbative interactions are dynamically cut off at the scale $\sim e_3^2$ in ultraviolet. Also, its dynamics is more efficient in generating a dynamical gap. Indeed, it corresponds to the dynamics in the reduced QED₃₊₁ when the coupling constant e of the latter goes to infinity. This feature has been already established in relativistic reduced QED₃₊₁,⁹ with $v_F = c$.

E. Beyond instantaneous approximation

Let us now turn to the discussion of the reliability of the instantaneous approximation for the gap equation. In this approximation, the frequency dependence in the photon propagator is neglected. While it is certainly justified for its free (kinetic) part, it is not immediately clear how good it is for the polarization function.

Keeping the frequency dependence, the gap equation at zero T and μ takes the following form in Euclidean space [compare with Eq. (B7) in Appendix B 2]:

$$\Delta(\Omega, p) = \frac{e^2}{\varepsilon_0} \int \frac{d\omega d^2k}{(2\pi)^2} \frac{\Delta(\omega, k)}{\omega^2 + v_F^2 |\vec{k}|^2 + \Delta(\omega, k)^2} \times \frac{1}{|\vec{p} - \vec{k}| + \Pi(\Omega - \omega, \vec{p} - \vec{k})}, \quad (36)$$

where the approximate polarization function is

$$\Pi(\omega, \vec{k}) = \frac{\pi e^2 N_f}{4\varepsilon_0 v_F^2} \sqrt{\omega^2 + v_F^2 |\vec{k}|^2}. \quad (37)$$

In the instantaneous approximation, we used $\omega^2 \rightarrow 0$ in the polarization function. Thus, the strength of the interaction was somewhat overestimated in such an approximation.

Unfortunately, it is hard to solve integral equation (36) analytically. In order to get an insight into the reliability of the instantaneous approximation, we will consider an auxiliary integral equation obtained from Eq. (36) by replacing the free part of the photon propagator as

$$|\vec{p} - \vec{k}| \rightarrow \sqrt{|\vec{p} - \vec{k}|^2 + (\Omega - \omega)^2 / v_F^2}. \quad (38)$$

It is clear that this modification leads to an equation which *underestimates* the interaction strength. Therefore if the solution of this equation is similar to that of the equation in the instantaneous approximation (which *overestimates* the interaction strength), it would imply that the instantaneous approximation is good enough. As we shall show below, another use of this auxiliary equation is that it yields the same value for the critical value N_f^{cr} as the gap equation (36).

Using the modified Eq. (38) and changing the variables as follows:

$$\vec{k} \rightarrow \frac{1}{v_F} \vec{k}, \quad (39)$$

$$\omega \rightarrow k_3, \quad (40)$$

we arrive at the auxiliary equation

$$\Delta(p) = \frac{2\lambda}{\pi} \int_{\Delta_0}^{\infty} dk \Delta(k) \left(\frac{\theta(p-k)}{p} + \frac{\theta(k-p)}{k} \right), \quad (41)$$

where $k = \sqrt{\vec{k}^2 + k_3^2}$. This equation is the same as equation (21) except for the replacement

$$\lambda \rightarrow \frac{2\lambda}{\pi}. \quad (42)$$

Therefore the gap is now generated, provided that

$$\lambda > \frac{\pi}{8}, \quad (43)$$

which translates into

$$g_{cr} = \frac{4}{(16/\pi) - \pi N_f}. \quad (44)$$

This relation is quite close to relation (28), obtained in the instantaneous approximation. The only difference appears in the first term in the denominator which is $16/\pi$ instead of 8. This implies that the instantaneous approximation is reasonable indeed.

An interesting feature of the auxiliary equation (41) is that it coincides with the gap equation (36) in the limit $g \rightarrow \infty$. Indeed, these two equations differ only by the free (kinetic) part of the photon propagator, and this part becomes irrelevant as $g \rightarrow \infty$. On the other hand, in this limit, reduced QED₃₊₁ coincides with QED₂₊₁ and, therefore, the critical line (44) with $g_{cr} \rightarrow \infty$ determines the critical value N_f^{cr} in the latter model. We get

$$N_f^{cr} = \frac{16}{\pi^2} \approx 1.62. \quad (45)$$

Notice that this value is twice as small as $N_f^{cr} = 3.24$ obtained in relativistic QED₂₊₁, in a similar approximation.²⁵ This is of course connected with additional, retarded, forces present in the relativistic model.

Since in graphite $N_f = 2 > N_f^{cr} = 1.62$, the critical coupling equals $g_{cr} = \infty$ in the leading order in $1/N_f$. One should remember however that $1/N_f$ corrections could be relevant for the values of N_f of order 1. Using the argument in Ref. 24, one may expect the variations up to 50 percent in the value of N_f^{cr} . Therefore the value $N_f^{cr} = 1.62$, obtained here in leading order in $1/N_f$, should be considered just as a useful estimate.

IV. GAP EQUATION. NONZERO MAGNETIC FIELD

The main goal of this paper is the description of the magnetic field driven metal-insulator phase transition in planar systems. Having developed a general formalism in the preceding sections, here we will take into account the effect of an external magnetic field on the dynamics of a spontaneous generation of a gap. The general observation of Refs. 13,14 states that in the presence of an external magnetic field, there is the generation of a dynamical gap connected with electron-hole pairing even for an arbitrary weak attraction between electrons and holes. Therefore in this case the gap will appear even if the bare coupling constant g , introduced in the previous section, is subcritical (in the case of a supercritical g , the magnetic field would enhance the already existent gap). This phenomenon is known as ‘‘magnetic catalysis’’. The origin of this effect is connected with the dynamics of the LLL: its dynamics is effectively 0+1 (1+1) dimensional in 2+1 (3+1) dimensions and this makes the electron-hole pairing inevitable.

Actually, this formulation is correct only in the case of zero temperature and zero charge density. In the presence of temperature T and/or charge density n , there is a critical value of the magnetic field, $B_c(T, n)$, defining a threshold for this effect: B has to be larger than $B_c(T, n)$.¹³ While the dependence of $B_c(T, n)$ on T is model dependent, the value of $B_c(0, n)$ is universal for all values of $g \leq g_c$: it is given by $|e|B_c = 2\pi cn/N_f$ and corresponds to the filling of the lowest Landau level.¹³ The physics of this result is quite clear: when the LLL is filled up, the LLL electrons are blocked and excluded from the pairing dynamics. In other words, in this case we lose the catalyst and, therefore, the effect itself. As we will see in Sec. VI, this point can be crucial for explaining the presence of an offset field B_c observed in the recent experiments in highly oriented pyrolytic graphite.^{18–20}

A. Dynamical gap at $T = 0$ and $\mu = 0$

In a constant external magnetic field B , only the free part of the quasiparticle action is modified. In particular, the spatial derivatives in Eq. (5) are replaced by the corresponding covariant derivatives:

$$\partial_x \rightarrow \partial_x + i\frac{e}{c}A_x^{ext}(\vec{r}), \quad (46)$$

$$\partial_y \rightarrow \partial_y + i\frac{e}{c}A_y^{ext}(\vec{r}), \quad (47)$$

where $A_x^{ext}(\vec{r}) = -By/2$ and $A_y^{ext}(\vec{r}) = Bx/2$. In this case, the propagator of quasiparticles takes the following general form:^{14,27}

$$G(t - t', \vec{r}, \vec{r}') = \exp\left[-i\frac{e}{c}\vec{r} \cdot \vec{A}^{ext}(\vec{r}')\right] \tilde{G}(t - t', \vec{r} - \vec{r}'), \quad (48)$$

Notice that while we used the symbol S for the fermion propagator in the case without magnetic field, we use the symbol G for the fermion propagator in a magnetic field. Let us begin by considering the propagator of free quasiparticles in a magnetic field, $G_0(t - t', \vec{r}, \vec{r}')$. For our purposes, it will be useful to introduce the bare gap Δ_b for these free quasiparticles. The translation invariant part of such a propagator, $\tilde{G}_0(t - t', \vec{r} - \vec{r}')$, reads¹³

$$\begin{aligned} \tilde{G}_0(t, \vec{r}) &= \int \frac{dt}{2\pi} \frac{d^2\vec{k}}{(2\pi)^2} \exp(-i\omega t + i\vec{k} \cdot \vec{r}) \tilde{G}_0(\omega, \vec{k}), \quad (49) \\ \tilde{G}_0(\omega, \vec{k}) &= 2i \exp\left(-\frac{c|\vec{k}|^2}{|eB|}\right) \\ &\times \sum_{n=0}^{\infty} \frac{(-1)^n \left[(\omega\gamma^0 + \Delta_b)f_1(\vec{k}) + f_2(\vec{k})\right]}{\omega^2 - \Delta_b^2 - 2nv_F^2|eB|/c}. \quad (50) \end{aligned}$$

In this last equation, we used the shorthand notation:

$$f_1(\vec{k}) = \mathcal{P}_{-L_n} \left(\frac{2c\vec{k}^2}{|eB|} \right) - \mathcal{P}_{+L_{n-1}} \left(\frac{2c\vec{k}^2}{|eB|} \right), \quad (51)$$

$$f_2(\vec{k}) = 2v_F \vec{k} \vec{\gamma} L_{n-1}^1 \left(\frac{2c\vec{k}^2}{|eB|} \right). \quad (52)$$

with the following spin projection operators:

$$\mathcal{P}_{\pm} = \frac{1 \pm i\gamma^1\gamma^2}{2}. \quad (53)$$

Also, $L_n^\alpha(z)$ are the generalized Laguerre polynomials. By definition, $L_n(z) \equiv L_n^0(z)$ and $L_{-1}^\alpha(z) \equiv 0$.

Let us now turn to the interactions in the presence of the magnetic field. In this case the polarization effects could also be taken into account,²⁸ and the modified interaction is:

$$\begin{aligned} U(t, \vec{r}) &= \delta(t) \frac{e^2}{\varepsilon_0} \int \frac{d^2\vec{k}}{2\pi} \frac{\exp(i\vec{k} \cdot \vec{r})}{|\vec{k}|(1 + a|\vec{k}|)} \\ &= \frac{e^2\pi\delta(t)}{2\varepsilon_0 a} \left[H_0 \left(\frac{|\vec{r}|}{a} \right) - N_0 \left(\frac{|\vec{r}|}{a} \right) \right], \quad (54) \end{aligned}$$

where

$$a = 2\pi\nu_0 \frac{e^2 N_f}{\varepsilon_0 v_F} \sqrt{\frac{c}{|eB|}}, \quad (55)$$

and the constant ν_0 is given by

$$\begin{aligned}\nu_0 &\equiv \frac{1}{4\pi\sqrt{\pi}} \int_0^\infty \frac{dz}{\sqrt{z}} \left(\frac{\coth(z)}{z} - \frac{1}{\sinh^2(z)} \right) \\ &= -\frac{3\zeta(-0.5)}{\sqrt{2\pi}} \approx 0.14.\end{aligned}\quad (56)$$

Regarding the new notation, $\zeta(z)$ is the Riemann zeta function, $H_0(z)$ is the Struve function, and $N_0(z)$ is the Bessel function of the second kind. It is noticeable that the instantaneous approximation for the polarization function is justified in this case: the frequency dependence is suppressed by factors of order $\omega/\sqrt{v_F|eB|}$ (which are small in the case of the LLL dominance (see below)). This can be shown directly from the expression for the polarization function in Ref. 28.

Now, the gap equation for the quasiparticle propagator reads

$$\begin{aligned}\tilde{G}(t, \vec{r}) &= \tilde{G}_0(t, \vec{r}) - i \int dt' d^2\vec{r}' \int dt'' d^2\vec{r}'' \\ &\times \exp \left[-i\vec{r} \cdot \vec{A}(\vec{r}') - i\vec{r}' \cdot \vec{A}(\vec{r}'') \right] \\ &\times \tilde{G}_0(t-t', \vec{r}-\vec{r}') \gamma^0 \tilde{G}(t'-t'', \vec{r}'-\vec{r}'') \\ &\times \gamma^0 \tilde{G}(t'', \vec{r}'') U(\vec{r}'-\vec{r}'') \delta(t'-t'').\end{aligned}\quad (57)$$

The structure of this equation is essentially the same as in the relativistic model of Refs. 14,27. Here, however, we neglect the retardation effects in the interaction potential. When the Fermi velocity v_F is very small compared to the speed of light, this is justified.

As was pointed out in Ref. 13, in the case of a subcritical coupling constant $g \leq g_c$, one should distinguish two different dynamical regimes. The first regime corresponds to the situation with a weak coupling g , when it is outside the scaling region near the critical value g_c . In this case the LLL dominates and the value of the dynamical gap Δ_0 is much less than the gap $\sqrt{2v_F^2|eB|/c}$ between the Landau levels. The latter guarantees that the higher Landau levels decouple from the pairing dynamics and the LLL dominates indeed.

The second, strong coupling, regime is that with a near-critical, although subcritical, value of g . In that case, all Landau levels are relevant for the pairing dynamics and the value of the dynamical gap Δ_0 is of order of the Landau gap $\sqrt{2v_F^2|eB|/c}$.

Let us begin by considering the first regime. Then, the low energy dynamics is dominated by the LLL, and the quasiparticle propagator could be approximated as follows:

$$\tilde{G}(t, \vec{r}) = \frac{i|eB|}{4\pi c} \exp \left(-\frac{|\vec{r}|^2|eB|}{4c} \right) g(t)(1 - i\gamma^1\gamma^2), \quad (58)$$

where $g(t)$ is unknown matrix-valued function which should be determined by solving the Schwinger-Dyson equation. By substituting the ansatz (58) into Eq. (57), we derive the following equation for the Fourier transform of $g(t)$:

$$\begin{aligned}g^{-1}(\omega) &= g_0^{-1}(\omega) - ie^2 \int \frac{d\omega'}{2\pi} \gamma^0 g(\omega - \omega') \gamma^0 \\ &\times \int \frac{d^2\vec{k}}{(2\pi)^2} \exp \left[-\frac{c|\vec{k}|^2}{2|eB|} \right] U(\vec{k}).\end{aligned}\quad (59)$$

The value of the bare gap is now zero in the free propagator $g_0(\omega)$. And the general structure of the function $g(\omega)$ is suggested by the first (LLL) term in the bare propagator (50), where now the bare gap Δ_b should be replaced by the dynamical gap function Δ_ω and the wave function renormalization A_ω should be introduced. Thus, we have

$$g(\omega) = \frac{A_\omega \gamma^0 \omega + \Delta_\omega}{A_\omega^2 \omega^2 - \Delta_\omega^2}. \quad (60)$$

One could see that the integral on the right hand side of Eq. (59) is independent of ω . This implies that $A_\omega = 1$ and the gap Δ_ω is independent of ω . By taking this into account, we straightforwardly derive the solution:

$$\Delta_0 = \frac{g}{\sqrt{2}} \sqrt{\frac{v_F^2|eB|}{c}} \int_0^\infty \frac{dk \exp(-k^2)}{1 + k\chi_0}, \quad (61)$$

where

$$\chi_0 = 2\sqrt{2}\pi\nu_0 g N_f. \quad (62)$$

In two limiting cases, $\chi_0 \ll 1$ and $\chi_0 \gg 1$, we get the following asymptotes:

$$\Delta_0 \simeq \frac{g\sqrt{\pi}}{2\sqrt{2}} \sqrt{\frac{v_F^2|eB|}{c}} \left(1 - \frac{\chi_0}{\sqrt{\pi}} + \frac{\chi_0^2}{2} + \dots \right), \quad (63)$$

(for weak coupling and small N_f) and

$$\Delta_0 \simeq \frac{g}{\sqrt{2}} \sqrt{\frac{v_F^2|eB|}{c}} \frac{\ln \chi_0}{\chi_0} \equiv \frac{v_F}{4\pi\nu_0 N_f} \sqrt{\frac{|eB|}{c}} \ln \chi_0, \quad (64)$$

(for large N_f). In accordance with the general conclusion of Refs. 13,14, in a magnetic field the gap is generated for any nonzero coupling constant $g = e^2/\varepsilon_0 v_F$.

One can see that for a sufficiently small $g = e^2/\varepsilon_0 v_F$ in expression (63) and for a sufficiently large N_f in (64), the LLL approximation is selfconsistent indeed: in both cases, the gap Δ_0 can be made much less than the Landau gap (scale) $L \equiv \sqrt{2v_F^2|eB|/c}$. We emphasize that the second solution (64), obtained also in Ref. 7, corresponds to the regime with a large N_f and *not* to the strong coupling regime with a large g and N_f of order one. Indeed, taking g to be large enough in expression (64), one gets the gap Δ_0 exceeding the Landau scale L , i.e., for large g the self-consistency of the LLL dominance approximation is lost. We will discuss the strong coupling regime below.

What is the energy scale the coupling constant g relates to in this problem? It is the Landau scale L . The argument supporting this goes as follows. There are two, dynamically very different, scale regions in this problem.

One is the region with the energy scale above the Landau scale L and below the ultraviolet cutoff Λ , defined by the lattice size. In that region, the dynamics is essentially the same as in the theory without magnetic field. In particular, the running coupling decreases logarithmically with the energy scale there.⁶ Another is the region below the Landau scale. In that region, the magnetic field dramatically changes the dynamics, in particular, the behavior of the running coupling constant. As the analysis of this section shows, because of the magnetic field, the pairing dynamics (in the particle-hole channel) is dominated by the infrared region where $\omega \lesssim \Delta_0$. Therefore, the scale region above the Landau scale L completely decouples from the pairing dynamics in this case. This manifests itself in expression (61) for the gap: the only relevant scale is the Landau scale L there. Since the effect of the running of the coupling is taken into account by the polarization function in the gap equation, we conclude that the coupling g indeed relates to the Landau scale in this problem. Notice that it can be somewhat smaller than the bare coupling constant $g(\Lambda)$ related to the scale Λ . Taking $\Lambda = 2.4$ eV in graphite (the width of its energy band) and using the equation for the running coupling from Ref. 6, one gets that it is smaller by the factors 1.2 and 1.4 than $g(\Lambda)$ for the values of the magnetic field $B = 10$ T and $B = 0.1$ T, respectively.

Now let us turn to the second, strong coupling, dynamical regime. In reduced QED, the gap equation in this regime includes the contributions of all the Landau levels and becomes very formidable. Still, one can estimate the value of the gap: since there are no small parameters in this regime for moderate values of N_f , the gap should be of the order of the Landau scale L . This conclusion is supported by studying this regime in a simpler model, 2 + 1 dimensional Nambu-Jona-Lasinio model.¹³ In that case, in the critical regime, the gap equals $\Delta_0 \simeq 0.32L$, where the Landau scale in that relativistic model, with $v_F = c$, is $L = \sqrt{2c|eB|}$. As we will see in Sec. VI, the critical dynamical regime can be relevant for the magnetic field driven phase transition in highly oriented pyrolytic graphite.^{18–20}

B. Dynamical gap at $T \neq 0$ or $\mu \neq 0$

By making use of the Matsubara formalism, it is easy to generalize the gap equation for the case of a finite temperature and a nonzero chemical potential. Without going into all details, let us write down the final equation,

$$\Delta_T(\mu) = \frac{e^2}{2\sqrt{2}\varepsilon_0} \sqrt{\frac{|eB|}{c}} \int_0^\infty \frac{dk \exp(-k^2)}{1 + k\chi_0} \times \frac{\sinh \frac{\Delta_T(\mu)}{T}}{\cosh \frac{\Delta_T(\mu)}{T} + \cosh \frac{\mu}{T}}. \quad (65)$$

In the LLL dominance approximation, the expression for charge density of carriers in terms of the chemical poten-

tial is

$$n = \frac{N_f |eB|}{2\pi c} \frac{\sinh \frac{\mu}{T}}{\cosh \frac{\Delta_T(\mu)}{T} + \cosh \frac{\mu}{T}}. \quad (66)$$

We assume that, in the model at hand, the charge density of carriers (i.e., $n = n_{el} - n_h$) is a fixed constant. Then, the expression for the chemical potential reads

$$\sinh \frac{\mu}{T} = \frac{\nu_B}{1 - \nu_B^2} \left(\cosh \frac{\Delta_T(\mu)}{T} + \sqrt{1 + \nu_B^2 \sinh^2 \frac{\Delta_T(\mu)}{T}} \right), \quad (67)$$

$$\cosh \frac{\mu}{T} = \frac{1}{1 - \nu_B^2} \left(\sqrt{1 + \nu_B^2 \sinh^2 \frac{\Delta_T(\mu)}{T}} + \nu_B^2 \cosh \frac{\Delta_T(\mu)}{T} \right), \quad (68)$$

where

$$\nu_B = \frac{2\pi cn}{N_f |eB|} \equiv \frac{B_c}{B} \quad (69)$$

is the filling factor.

By making use of the expression for the chemical potential in terms of the filling factor ν_B , we rewrite the gap equation in the following convenient form:

$$\Delta_T(\nu_B) = \frac{e^2}{2\sqrt{2}\varepsilon_0} \sqrt{\frac{|eB|}{c}} \int_0^\infty \frac{dk \exp(-k^2)}{1 + k\chi_0} \times \frac{(1 - \nu_B^2) \sinh \frac{\Delta_T(\nu_B)}{T}}{\cosh \frac{\Delta_T(\nu_B)}{T} + \sqrt{1 + \nu_B^2 \sinh^2 \frac{\Delta_T(\nu_B)}{T}}}. \quad (70)$$

Let us first consider the case of zero temperature. Then the gap equation takes a very simple form:

$$\Delta_0(\nu_B) = \frac{1 - \nu_B}{2} \Delta_0 \equiv \frac{e^2(1 - \nu_B)}{2\sqrt{2}\varepsilon_0} \sqrt{\frac{|eB|}{c}} \int_0^\infty \frac{dk \exp(-k^2)}{1 + k\chi_0}, \quad (71)$$

where $\Delta_0 \equiv \Delta_0(0)$ is the value of the gap at the zero filling factor. Since we choose the vacuum in which the gap is positive (see Sec. III A), this equation implies that for $\nu_B \geq 1$, there is no solution with a nonzero gap, i.e. the symmetry is restored. The condition $\nu_B = 1$ determines the critical density, $n_c = N_f |eB|/2\pi c$. The density n_c corresponds to the filling of the LLL and, as was discussed at the beginning of this section, this value is universal for all subcritical values of the coupling constant g . Reversing the roles of n and B , one can say that, for a fixed value of the density n , the critical value of the magnetic field is $|eB_c| = 2\pi cn/N_f$: a dynamical gap occurs only for magnetic fields B larger than B_c .

The critical temperature is determined from Eq. (70) with $\Delta_T(\nu_B) = 0$:

$$T_c = \frac{e^2(1 - \nu_B^2)}{4\sqrt{2}\varepsilon_0} \sqrt{\frac{|eB|}{c}} \int_0^\infty \frac{dk \exp(-k^2)}{1 + k\chi_0}. \quad (72)$$

At a fixed density n , this equation implies that, as it should be, the critical temperature is zero for magnetic fields weaker than the critical value B_c determined above. For magnetic fields B stronger than B_c , T_c grows with B (see Fig. 9 in Sec. VI). As we will see in Sec. VI, these results can be important for explaining experimental data in highly oriented pyrolytic graphite.^{18–20}

Though here we considered only the dynamical regime with the LLL dominance, it is reasonable to assume that the qualitative picture will remain the same also in the case of the scaling dynamical regime, with the near-critical coupling constant g . This is in particular supported by the fact of the universality of the critical value B_c .

Before concluding this section, let us mention that the the gap equation could also be rewritten in the following form:

$$\Delta_T(\nu_B) = \frac{2T_c \sinh \frac{\Delta_T(\nu_B)}{T}}{\cosh \frac{\Delta_T(\nu_B)}{T} + \sqrt{1 + \nu_B^2 \sinh^2 \frac{\Delta_T(\nu_B)}{T}}}, \quad (73)$$

where the relation (72) was taken into account. The last form of the gap equation will be the most convenient for using in numerical calculations of conductivity, see Sec. VB.

V. CONDUCTIVITY AND RESISTIVITY

Conductivity and resistivity are major players in experimental detecting the magnetic field driven semimetal-insulator phase transition in graphite.^{18–20} In this section, we will calculate them in reduced QED₃₊₁ with a 2-brane using the results obtained in the previous sections. We will consider both cases of zero and nonzero external magnetic fields. While the former case is interesting in itself, it will also serve us as an important reference point for the latter. The main conclusion of this section is that there is a clear signature of the phase transition seen in the behavior of the conductivity (resistivity) as a function of temperature. More precisely, we find that

1. if the phase transition is of the first order, there is a discontinuity in the conductivity (resistivity) at a critical temperature T_c ;
2. if the phase transition is of the second order and the scaling properties are correctly described by the mean-field approximation, the conductivity (resistivity) exhibits a kink behavior at the critical temperature;

3. at last, if the phase transition is a continuous higher order one, the conductivity (resistivity) is a smooth function at the critical temperature T_c , while a singularity occurs in its higher derivatives at $T = T_c$.

Besides, our calculations show that in this particular model, the flavor phase transition, restoring the flavor symmetry $U(2N_F)$, does not look as a semimetal-insulator phase transition *if* there is no external magnetic field. On the other hand, in the presence of a magnetic field, in many cases it does look as a semimetal-insulator phase transition.

A. No Magnetic Field

In calculation of transport coefficients, it is very useful to utilize the spectral representation of the quasiparticle Green function. The latter is defined as follows:²⁹

$$S(i\omega_n, \vec{k}) = i \int_{-\infty}^{\infty} \frac{d\omega A(\omega, \vec{k})}{i\omega_n - \mu - \omega}. \quad (74)$$

In the reduced planar model described in Sec. II, we derive

$$A(\omega, \vec{k}) = \frac{\Gamma}{2\pi E} \left[\frac{\gamma^0 E - \vec{k}\vec{\gamma} + \Delta}{(\omega - E)^2 + \Gamma^2} + \frac{\gamma^0 E + \vec{k}\vec{\gamma} - \Delta}{(\omega + E)^2 + \Gamma^2} \right], \quad (75)$$

where $E = \sqrt{v_F^2 k^2 + \Delta^2}$ and, throughout this section, we use the symbol Δ for the gap, i.e., $\Delta \equiv \Delta_T(\mu)$ and $\Delta \equiv \Delta_T(\nu_B)$ for the cases with no and with magnetic field, respectively. Notice that we introduced a phenomenological width parameter Γ without which the calculation of conductivities would be meaningless. A finite width parameter appears as a result of interactions, and scattering on impurities, in particular. In general, the width Γ is defined through the fermion self-energy as $\Gamma(\omega) = -\text{Im}\Sigma^R(\omega)$. Thus, it is a frequency (as well as temperature and magnetic field) dependent quantity. Like the dynamical gap itself, it should be self-consistently determined from the Schwinger-Dyson equations. At low temperatures, usually it could be modeled by a constant phenomenological parameter. Therefore, instead of considering an additional Schwinger-Dyson type equation, we choose a constant parameter Γ and view this as yet another approximation.

In terms of the spectral function, the charge density of carriers reads

$$n = \frac{1}{2} \int \frac{d^2k}{(2\pi)^2} \int_{-\infty}^{\infty} d\omega \left(\tanh \frac{\omega + \mu}{2T} - 1 \right) \text{tr} \left[\gamma^0 A(\omega, \vec{k}) \right]. \quad (76)$$

The conductivity tensor is defined as follows:

$$\sigma_{ij} = \lim_{\Omega \rightarrow 0} \frac{\text{Im}\Pi_{ij}^R(\Omega + i\epsilon)}{\Omega}, \quad (77)$$

where $\Pi_{ij}^R(\Omega)$ is the retarded current-current correlation function which is also given in terms of the spectral function,

$$\begin{aligned} \Pi_{ij}(\Omega + i\epsilon) &= \frac{e^2 v_F^2}{2} \int_{-\infty}^{\infty} d\omega d\omega' \frac{\tanh \frac{\omega+\mu}{2T} - \tanh \frac{\omega'+\mu}{2T}}{\omega - \omega' + \Omega + i\epsilon} \\ &\times \int \frac{d^2k}{(2\pi)^2} \text{tr} \left[\gamma_i A(\omega, \vec{k}) \gamma_j A(\omega', \vec{k}) \right]. \end{aligned} \quad (78)$$

The vertex corrections were neglected in this expression. Formally, they are suppressed by a power of $1/N_f$. Of course, in the case of graphite (with $N_f = 2$), the vertex contributions may nevertheless play an important role.³⁰ This question should be studied in more detail, but it is outside the scope of the present paper. In absence of a magnetic field, the conductivity tensor has only the diagonal components, $\sigma = \sigma_{xx} = \sigma_{yy}$. Both components are equal as a result of rotational invariance of the model. The explicit expression of the conductivity, in this case, reads

$$\begin{aligned} \sigma &= \frac{e^2 N_f}{4\pi^2 T} \int_{-\infty}^{\infty} \frac{\Gamma^2 d\omega}{\cosh^2 \frac{\omega+\mu}{2T}} \int_{\Delta^2}^{\infty} dx \frac{(x + \omega^2 + \Gamma^2)^2 - 4\omega^2 \Delta^2}{[(x + \omega^2 + \Gamma^2)^2 - 4x\omega^2]^2} \\ &= \frac{e^2 N_f}{8\pi^2 T} \int_{-\infty}^{\infty} \frac{d\omega}{\cosh^2 \frac{\omega+\mu}{2T}} \left[1 + \frac{\omega^2 - \Delta^2 + \Gamma^2}{2|\omega|\Gamma} \right. \\ &\times \left. \left(\frac{\pi}{2} - \arctan \frac{\Gamma^2 + \Delta^2 - \omega^2}{2|\omega|\Gamma} \right) \right], \end{aligned} \quad (79)$$

where Γ is the width parameter, and the density of carriers is defined by the following relation:

$$\begin{aligned} n &= \frac{\Gamma N_f}{2\pi^2 v_F^2} \int_{-\infty}^{\infty} \frac{d\omega}{\omega^2 + \Gamma^2} \int_{\Delta}^{\infty} dEE \\ &\times \left[\tanh \frac{\omega + \mu + E}{2T} + \tanh \frac{\omega + \mu - E}{2T} \right]. \end{aligned} \quad (80)$$

In the limit $\Gamma \rightarrow 0$, these two expressions reduce to

$$\begin{aligned} \sigma &= \frac{e^2 N_f}{16\pi T \Gamma} \int_{-\infty}^{\infty} \frac{d\omega}{\cosh^2 \frac{\omega+\mu}{2T}} \frac{\omega^2 - \Delta^2}{|\omega|} \theta(\omega^2 - \Delta^2) \\ &= \frac{e^2 N_f}{16\pi T \Gamma} \int_{\Delta}^{\infty} \frac{d\omega}{\omega} \left[\frac{\omega^2 - \Delta^2}{\cosh^2 \frac{\omega+\mu}{2T}} + (\mu \rightarrow -\mu) \right], \end{aligned} \quad (81)$$

and

$$n = \frac{N_f}{2\pi v_F^2} \int_{\Delta}^{\infty} dEE \left[\tanh \frac{\mu + E}{2T} + \tanh \frac{\mu - E}{2T} \right]$$

$$\begin{aligned} &= \frac{N_f T^2 \sinh \frac{\mu}{T}}{\pi v_F^2} \int_{\frac{\mu}{T}}^{\infty} \frac{dx x}{\cosh x + \cosh \frac{\mu}{T}} \\ &= \frac{N_f T^2}{\pi v_F^2} \left[\frac{\Delta}{T} \ln \frac{1 + \exp(\frac{\mu-\Delta}{T})}{1 + \exp(-\frac{\mu+\Delta}{T})} \right. \\ &\left. + \text{Li}_2 \left(-e^{-\frac{\mu+\Delta}{T}} \right) - \text{Li}_2 \left(-e^{-\frac{\mu-\Delta}{T}} \right) \right], \end{aligned} \quad (82)$$

where $\text{Li}_2(z)$ is the dilogarithm function. As one could see from the above formulas, the conductivity grows linearly with temperature when the temperature is large,

$$\sigma \simeq \frac{e^2 N_f T}{4\pi \Gamma} \ln 2, \quad \text{for } T \rightarrow \infty. \quad (83)$$

Notice, however, that the expression for the conductivity in Eq. (81), derived for the $\Gamma \rightarrow 0$ case, fails when temperatures become very small. The correct result for small temperatures could be derived from Eq. (79). It reads

$$\begin{aligned} \sigma &= \frac{e^2 N_f}{2\pi^2} \left[1 + \frac{\mu^2 - \Delta^2 + \Gamma^2}{2|\mu|\Gamma} \right. \\ &\times \left. \left(\frac{\pi}{2} - \arctan \frac{\Gamma^2 + \Delta^2 - \mu^2}{2|\mu|\Gamma} \right) + O\left(\frac{T}{\Gamma}\right) \right]. \end{aligned} \quad (84)$$

The density in that same limit is

$$n = \frac{N_f}{2\pi v_F^2} (\mu^2 - \Delta^2) \text{sgn}(\mu) \theta(\mu^2 - \Delta^2). \quad (85)$$

The interplay between the density of carriers and the width Γ is characterized by the following dimensionless parameter:

$$\eta = \frac{1}{\Gamma} \sqrt{\frac{2\pi v_F^2 n}{N_f}}. \quad (86)$$

In the two opposite limits of a clean or dirty system, this parameter is either large or small, respectively. Then, the corresponding zero temperature asymptotes for the conductivity take the form:

$$\sigma = \frac{e^2 N_f \eta}{4\pi} \sqrt{\frac{2\pi v_F^2 n}{2\pi v_F^2 n + N_f \Delta^2}}, \quad (87)$$

for $\eta \gg 1$, and

$$\sigma = \frac{e^2 N_f}{2\pi^2} \left[1 + \frac{\Gamma}{2\Delta} \left(\frac{\pi}{2} - \arctan \frac{\Gamma}{2\Delta} \right) \right], \quad (88)$$

for $\eta \ll 1$. The last expression was derived under the assumption that $n \ll \Delta^2/v_F^2$. Finally, in the strict limit of zero density (i.e., $\mu = 0$), we derive

$$\sigma = \frac{e^2 N_f}{\pi^2} \frac{\Gamma^2}{\Gamma^2 + \Delta^2}. \quad (89)$$

It should be emphasized that the strict case of zero density corresponds to $\mu = 0$ (rather than $\mu = \Delta$ as might be suggested by taking the limit $T \rightarrow 0$ first, and then $n \rightarrow 0$). To understand this better, one should look at the temperature dependence of the chemical potential at a given fixed value of the density. In particular, when the density of carriers is very small, the chemical potential as a function of temperature sharply falls from its value $\mu = \Delta$ at $T = 0$ almost down to zero in a very small region of temperatures. Afterwards, it starts to grow. When the density gets vanishingly small, the before mentioned region of temperatures where the chemical potential drops shrinks to zero. Thus, by making use of continuity argument, it is clear that the value of the chemical potential is zero in the limit $T \rightarrow 0$ if the density of carriers is zero.

It is noticeable that our result in Eq. (89) is in agreement with the Wiedemann-Franz law, i.e.,

$$\frac{\sigma T}{\kappa} \Big|_{T \rightarrow 0} = \frac{3e^2}{\pi^2}, \quad (90)$$

where we use the value of the thermal conductivity κ calculated in Ref. 31.

The numerical results for the temperature dependence of the conductivity are shown in Fig. 3 in the case of the zero gap (bold solid line), and nonzero gaps (other lines correspond to different values of T_c). Notice that the model at hand reveals an “insulator” (i.e., increasing with temperature) type dependence of conductivity even in the case of a finite density of carriers. This type of behavior is the consequence of using a constant value of the width parameter Γ in our model. Then, the growth of conductivity with increasing temperature is directly related to the increasing number of thermally excited quasiparticles. In realistic systems, of course, the width (which is related to the inverse scattering time) would normally start to grow with temperature too. In general, one might choose the width as function of energy and temperature,

$$\Gamma(\omega, T) = \Gamma_0 + \frac{1}{\tau(\omega, T)}, \quad (91)$$

where Γ_0 is the zero temperature width due to impurities, and the other term is due to the thermal contribution. In this paper, for the sake of simplicity, we consider the simplest model with a fixed constant value of the width parameter. The analysis, however, could be easily generalized for any phenomenologically motivated dependencies like that in Eq. (91).

In order to calculate the conductivities in the case of nonzero dynamical gaps, we used the gap equation (73) in which the critical temperature T_c was treated as a free parameter.

The results for the temperature dependence of the resistivity are plotted in Fig. 4.

As one can see in Fig. 3 and Fig. 4, there is a kink at the critical point $T = T_c$ in the conductivity (resistivity).

Its occurrence is directly related to the mean field behavior of the gap Δ in the vicinity of the critical point, i.e., $\Delta \sim \sqrt{T_c - T}$. Indeed, as follows from Eq. (79), the conductivity σ depends on Δ^2 and, therefore, its derivative with respect to temperature has a finite discontinuity at the critical point $T = T_c$.

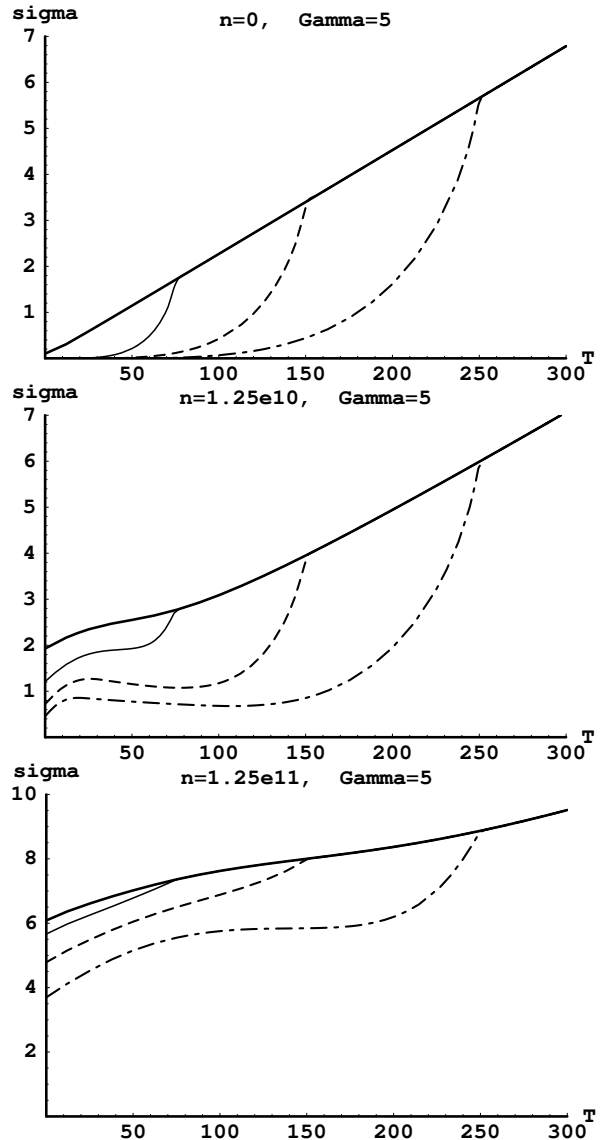


FIG. 3. The conductivity as a function of temperature for the zero magnetic field case. The bold solid line corresponds to the case without a gap. The other lines correspond to nonzero dynamical gaps and different values of T_c . Conductivity is measured in units of e^2 , both temperature and width Γ are measured in Kelvin, and density n is measured in cm^{-3} .

The mean field behavior may change if higher order, $1/N_f$, corrections (fluctuations) are taken into account. The fluctuations could either change the phase transition to a first order one, with a discontinuity in Δ at the phase transition point, or to a higher order phase transition, with the scaling law $\Delta \sim (T_c - T)^\nu$ where $\nu > 1/2$. While in the former case a discontinuity will

appear in the conductivity (resistivity), in the latter case the conductivity (resistivity) will be a smooth function of temperature, and a singularity will move to its higher derivatives.

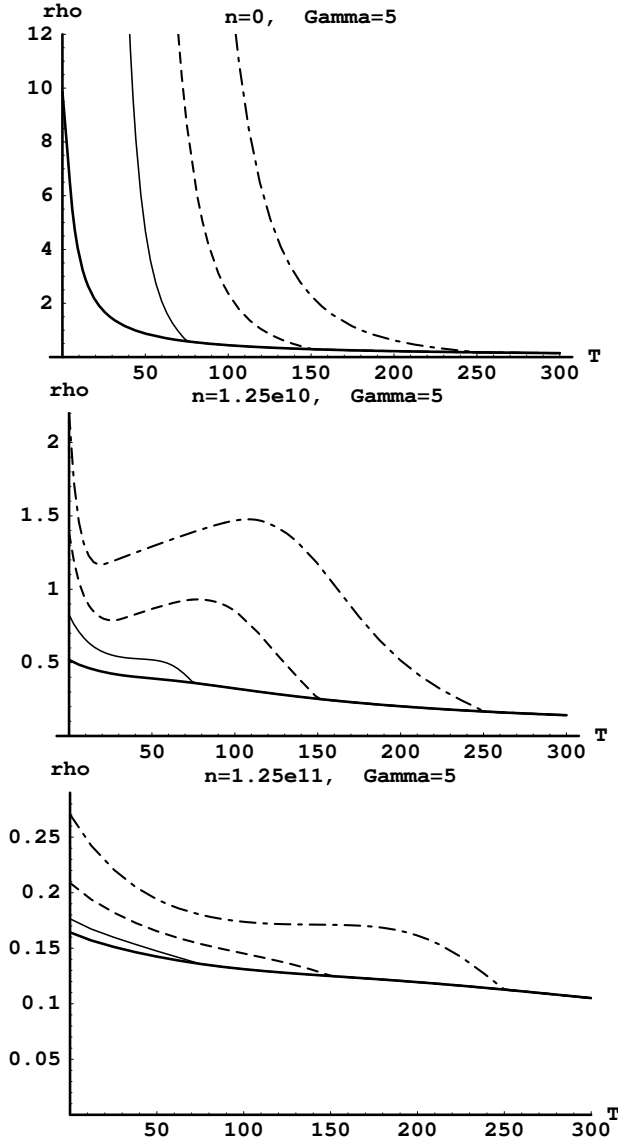


FIG. 4. The resistivity as a function of temperature for the zero magnetic field case. The bold solid line corresponds to the case without a gap. The other lines correspond to nonzero dynamical gaps and different values of T_c . Resistivity is measured in units of e^{-2} , both temperature and width Γ are measured in Kelvin, and density n is measured in cm^{-2} .

Another noticeable point is that in the case with no magnetic field, the flavor phase transition does *not* look as a semimetal-insulator one. Indeed, as one can see in Fig. 3 and Fig. 4, an “insulator” type behavior does not change at the critical point. As we will see in the next subsections, the occurrence of a magnetic field will drastically change this feature of the phase transition.

Before concluding this section, let us also mention that the conductivity (as well as the resistivity) become more

sensitive to the appearance of a dynamical gap when the density of carriers decreases. To support this statement, we plotted the conductivity and resistivity for two different finite values of carrier densities which differ by a factor 10, see lower parts of Figs. 3 and 4.

As we see from Fig. 4, the temperature dependence of the resistivity develops a minimum when the value of the gap is sufficiently large. Comparing this temperature dependence with the experimental data, we might even suggest that the studied graphite samples are better described by the model with a nonzero dynamical gap even in absence of a magnetic field. The effect of an external field is studied in the following subsections.

B. Conductivity tensor. Nonzero magnetic field.

Let us now turn to the analysis of the conductivity in the case with an external magnetic field. The spectral function $A(\omega, \vec{k})$ of the translation invariant part of the quasiparticle propagator in a magnetic field [see Eqs. (49) and (50)] is given by

$$A(\omega, \vec{k}) = \frac{\Gamma}{\pi} \exp\left(-\frac{c|\vec{k}|^2}{|eB|}\right) \sum_{n=0}^{\infty} \frac{(-1)^n}{M_n} \times \left[\frac{(\gamma^0 M_n + \Delta) f_1(\vec{k}) + f_2(\vec{k})}{(\omega - M_n)^2 + \Gamma^2} + \frac{(\gamma^0 M_n - \Delta) f_1(\vec{k}) - f_2(\vec{k})}{(\omega + M_n)^2 + \Gamma^2} \right], \quad (92)$$

where the functions $f_1(\vec{k})$ and $f_2(\vec{k})$ were defined earlier in Eqs. (51) and (52). In an external magnetic field, the conductivity is a tensor quantity. The diagonal and off-diagonal components of conductivity read

$$\sigma_{xx} = \frac{e^2 N_f |eB| \Gamma^2}{2\pi^2 T} \sum_{n=0}^{\infty} \int_{-\infty}^{\infty} \frac{d\omega}{\cosh^2 \frac{\omega + \mu}{2T}} \times \frac{(\omega^2 + M_n^2 + \Gamma^2)(\omega^2 + M_{n+1}^2 + \Gamma^2) - 4\omega^2 \Delta^2}{[(\omega^2 - M_n^2 - \Gamma^2)^2 + 4\omega^2 \Gamma^2][(\omega^2 - M_{n+1}^2 - \Gamma^2)^2 + 4\omega^2 \Gamma^2]}, \quad (93)$$

and

$$\sigma_{xy} = \frac{e^2 N_f}{2\pi} \nu_B, \quad (94)$$

respectively. Here the parameter Γ gives the energy width of Landau levels, and the filling factor ν_B [related to the density of carriers by the relation: $\nu_B = 2\pi cn/(N_f |eB|)$] is defined as follows:

$$\nu_B = \int_{-\infty}^{\infty} \frac{d\omega}{2\pi} \tanh \frac{\mu + \omega}{2T} \left[\frac{\Gamma}{(\omega - \Delta)^2 + \Gamma^2} + (\omega \rightarrow -\omega) + 2 \sum_{n=1}^{\infty} \left(\frac{\Gamma}{(\omega - M_n)^2 + \Gamma^2} + (\omega \rightarrow -\omega) \right) \right]. \quad (95)$$

The sum over Landau levels in Eq. (93) could be performed explicitly, and the result is given in terms of the digamma function, $\psi(z)$, as follows:

$$\begin{aligned} \sigma_{xx} = & \frac{e^2 N_f \Gamma}{4\pi^2 T} \int_{-\infty}^{\infty} \frac{d\omega}{\cosh^2 \frac{\omega + \mu}{2T}} \frac{\Gamma}{\left(\frac{v_F^2 e B}{c}\right)^2 + (2\omega\Gamma)^2} \left[2\omega^2 \right. \\ & + \frac{(\omega^2 + \Delta^2 + \Gamma^2) \left(\frac{v_F^2 e B}{c}\right)^2 - 2\omega^2(\omega^2 - \Delta^2 + \Gamma^2) \frac{v_F^2 e B}{c}}{(\omega^2 - \Delta^2 - \Gamma^2)^2 + 4\omega^2 \Gamma^2} \\ & \left. - \frac{\omega(\omega^2 - \Delta^2 + \Gamma^2)}{\Gamma} \text{Im} \psi \left(\frac{\Delta^2 + \Gamma^2 - \omega^2 - 2i\omega\Gamma}{2v_F^2 |eB|/c} \right) \right]. \end{aligned} \quad (96)$$

The high temperature asymptote that follows from the representation in Eq. (96) is the same as in the case of zero magnetic field, given in Eq. (83). The limit $T \rightarrow 0$ is different from that in Eq. (84). It is given by the following expression:

$$\begin{aligned} \sigma_{xx} = & \frac{e^2 N_f \Gamma}{\pi^2} \frac{\Gamma}{\left(\frac{v_F^2 e B}{c}\right)^2 + (2\mu\Gamma)^2} \left[2\mu^2 \right. \\ & + \frac{(\mu^2 + \Delta^2 + \Gamma^2) \left(\frac{v_F^2 e B}{c}\right)^2 - 2\mu^2(\mu^2 - \Delta^2 + \Gamma^2) \frac{v_F^2 e B}{c}}{(\mu^2 - \Delta^2 - \Gamma^2)^2 + 4\mu^2 \Gamma^2} \\ & \left. + \frac{\mu(\mu^2 - \Delta^2 + \Gamma^2)}{\Gamma} \text{Im} \psi \left(\frac{\Delta^2 + \Gamma^2 - \mu^2 + 2i\mu\Gamma}{2v_F^2 |eB|/c} \right) \right]. \end{aligned} \quad (97)$$

It is interesting to note, however, that for zero value of the gap and zero density of carriers (i.e., $\Delta = 0$ and $\mu = 0$), this last expression becomes identical with the expression for the conductivity in absence of a magnetic field given in Eq. (89).

In the limit of narrow width, $\Gamma \rightarrow 0$, the above expressions reduce down to

$$\begin{aligned} \sigma_{xx} = & \frac{e^2 N_f \Gamma}{2\pi T} \left[\frac{1 + \cosh \frac{\Delta}{T} \cosh \frac{\mu}{T}}{\left(\cosh \frac{\Delta}{T} + \cosh \frac{\mu}{T}\right)^2} \right. \\ & \left. + 4 \sum_{n=1}^{\infty} \frac{n(1 + \cosh \frac{M_n}{T} \cosh \frac{\mu}{T})}{\left(\cosh \frac{M_n}{T} + \cosh \frac{\mu}{T}\right)^2} \right], \end{aligned} \quad (98)$$

for diagonal component of the conductivity, and

$$\begin{aligned} \nu_B = & \frac{1}{2} \left(\tanh \frac{\mu + \Delta}{2T} + \tanh \frac{\mu - \Delta}{2T} \right) \\ & + \sum_{n=1}^{\infty} \left(\tanh \frac{\mu + M_n}{2T} + \tanh \frac{\mu - M_n}{2T} \right), \end{aligned} \quad (99)$$

for the filling factor.

In order to understand the effect of a dynamical gap on the behavior of conductivity as a function of temperature, it is helpful to start from the case of a vanishing density of carriers (i.e., $\nu_B = 0$). When $\nu_B = 0$, the Hall

conductivity is absent, and the resistivity is determined by σ_{xx} component alone. The plot of the conductivity as a function of temperature is given in Fig. 5.

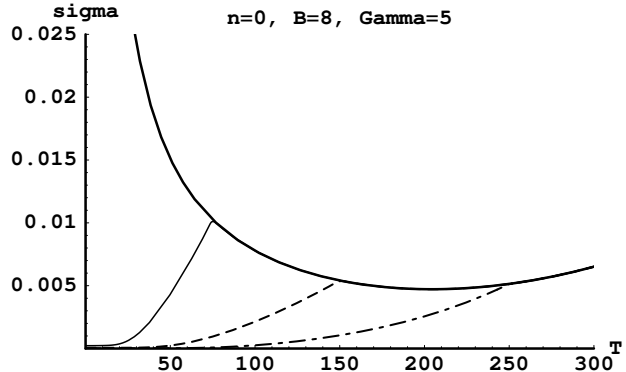


FIG. 5. The diagonal component of conductivity as a function of temperature for zero value of carrier density and a nonzero magnetic field, $B = 8$ Tesla. The bold solid line corresponds to the case without a gap. Other lines correspond to nonzero dynamical gaps and different values of T_c . Conductivity is measured in units of e^2 , both temperature and width Γ are measured in Kelvin.

The bold solid line corresponds to the case without a dynamical gap, while the other lines correspond to different choices of the gap magnitude. In the numerical analysis, we used the gap equation in Eq. (73), keeping the value of T_c as a free parameter.

When there are no free carriers, the low temperature dependence of the diagonal component of conductivity is very sensitive to the presence of a gap. In absence of a gap, the conductivity becomes infinitely large when $T \rightarrow 0$. At the same time, it is zero in the same limit when there is even an arbitrarily small gap Δ .

An important fact is that, unlike the case without magnetic field, the conductivity exhibits a (semi)metallic type behavior for zero gap and not too high temperatures ($T \lesssim 200$ K in Fig. 5). As a result, for not too large values of the critical temperature T_c ($T_c \lesssim 200$ K in Fig. 5), the flavor phase transition looks as a conventional semimetal-insulator one, when the insulator type behavior below T_c (nonzero gap) is replaced by the metallic type in a range of temperatures just above T_c (zero gap) (see Fig. 5).

A typical conductivity for a nonzero value of the filling factor ν_B (i.e., nonzero charge density) is shown in Fig. 6. In this case, the behaviors of the conductivity for a nonzero gap and zero gap are more similar than in the case of $\nu_B = 0$ (compare with Fig. 5). The presence of a gap, however, can substantially reduce the value of conductivity in the whole range of temperatures below T_c . It is important that, like in the case with $\nu_B = 0$, the flavor phase transition looks as a semimetal-insulator one for not too large values of the critical temperature T_c (see Fig. 6). It is the most important conclusion of this subsection.

The same arguments as in the end of Sec. V A show

that the occurrence of the kink in the conductivity at $T = T_c$ reflects the mean field behavior of the gap in the vicinity of the critical point, $\Delta \sim \sqrt{T_c - T}$. The $1/N_f$ fluctuations may change the character of the phase transition, leading either to a discontinuity in the conductivity $\sigma(T)$ at $T = T_c$ (a first order phase transition) or to a smooth function $\sigma(T)$ (a higher order continuous phase transition).

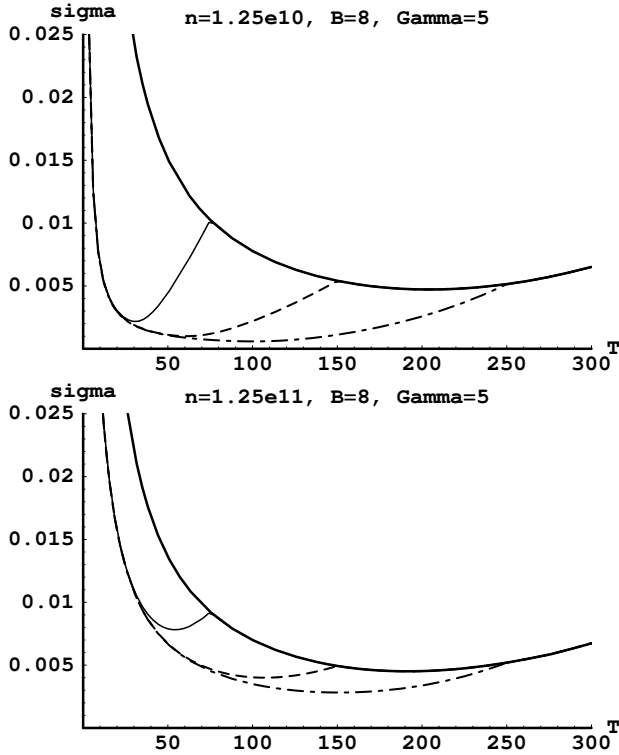


FIG. 6. The diagonal component of conductivity as a function of temperature for two different densities and a nonzero magnetic field, $B = 8$ Tesla. The bold solid line corresponds to the case without a gap. Other lines correspond to nonzero dynamical gaps and different values of T_c . Conductivity is measured in units of e^2 , both temperature and width Γ are measured in Kelvin, and density n is measured in cm^{-2} .

C. Resistivity tensor

In this subsection, we study the temperature dependence of the resistivity.

In terms of conductivities, the diagonal component of the resistivity reads

$$\rho_{xx} = \frac{\sigma_{xx}}{\sigma_{xx}^2 + \sigma_{xy}^2}. \quad (100)$$

In order to understand the general behavior of the resistivity, below we perform a set of numerical calculations.

Before presenting the results, it is instructive to notice that there exist two opposite regimes of dynamics controlled by the value of the charge density. In particular, at small density, when the Hall conductivity σ_{xy} is

negligible compared to σ_{xx} , the resistivity in Eq. (100) behaves as $1/\sigma_{xx}$. On the other hand, at sufficiently large density, when the Hall conductivity dominates over the diagonal component, the resistivity $\rho_{xx} \approx \sigma_{xx}/\sigma_{xy}^2$. By recalling that the Hall conductivity [see Eq. (94)] is independent of temperature, the general features of the temperature dependence of ρ_{xx} will be the same as of $1/\sigma_{xx}$ and σ_{xx} in the mentioned two regimes, respectively.

Now, let us present the numerical results. We begin by considering the case of zero density. In this case the Hall conductivity equals zero and the resistivity ρ_{xx} equals $1/\sigma_{xx}$. The temperature dependence of the resistivity is shown in Fig. 7 (compare with Fig. 5).

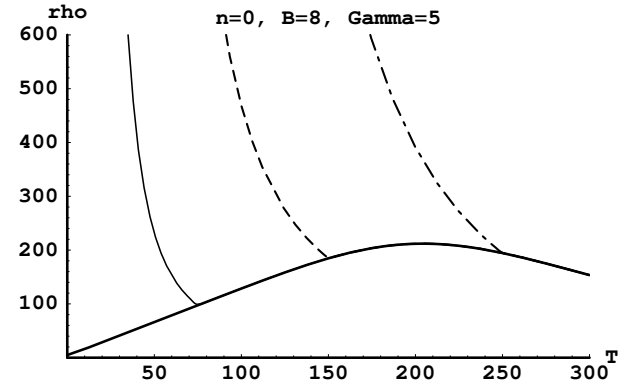


FIG. 7. The resistivity as a function of temperature for zero value of carrier density and a nonzero magnetic field, $B = 8$ Tesla. The bold solid line corresponds to the case without a gap. Other lines correspond to nonzero dynamical gaps and different values of T_c . Resistivity is measured in units of e^{-2} , both temperature and width Γ are measured in Kelvin.

The bold solid line corresponds to a model with the vanishing dynamical gap in the quasiparticle spectrum. The other curves correspond to three different choices of the dynamical gap. The temperature dependence of the dynamical gap is given by the gap equation (73) where the value of T_c was treated as a phenomenological parameter.

As one can see in Fig. 7, for zero dynamical gap (the bold solid line) the resistivity has a metallic type behavior for not too high temperatures ($T \lesssim 0.2v_F\sqrt{|eB|/c}$) and an insulator type behavior at high temperatures ($T \gtrsim 0.2v_F\sqrt{|eB|/c}$). This type of temperature dependence is driven by the magnetic field alone and is not related to the generation of a dynamical gap. Such a crossover from the metallic type behavior (low temperatures) to the insulator one (high temperatures) can be easily distinguished from the flavor phase transition taking place at not too high T_c . Indeed, when $T_c \lesssim 0.2v_F\sqrt{|eB|/c}$, one can see from Fig. 7 that it corresponds to the opposite, conventional, transition, when the insulator type behavior below T_c (nonzero gap) is replaced by the metallic type in a range of temperatures just above T_c (zero gap).

Let us now proceed to the case of a nonzero charge

density. As we mentioned at the beginning of this subsection, there are two different regimes that appear in the limits of small and large densities, respectively. Our results in Fig. 8 illustrate these regimes.

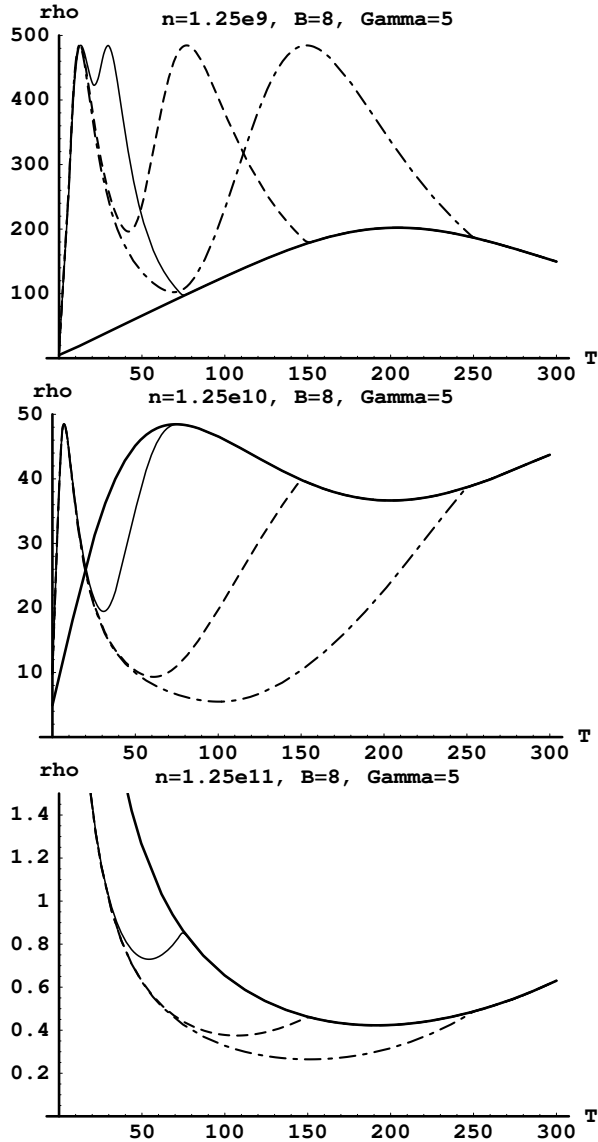


FIG. 8. The diagonal component of resistivity as a function of temperature for four different densities and a nonzero magnetic field, $B = 8$ Tesla. The bold solid line corresponds to the case without a gap. Other lines correspond to nonzero dynamical gaps and different values of T_c . Resistivity is measured in units of e^{-2} , both temperature and width Γ are measured in Kelvin, and density n is measured in cm^{-2} .

At small density (see the upper panel in Fig. 8), the resistivity behaves as $1/\sigma_{xx}$ almost at all temperatures (compare with Fig. 6), except for a finite region where σ_{xx} becomes very small due to the generation of a dynamical gap. In this region, even a small value of the Hall conductivity could dominate over σ_{xx} . This is seen as the appearance of a local minimum (between two maxima) in the temperature dependence of the resistivity. Of course,

in the absence of a dynamical gap (see the solid line in the upper panel in Fig. 8), the resistivity remains essentially the same as that at $n = 0$ (compare with Fig. 7).

This picture changes dramatically with increasing the density. As one can see in the two lower panels in Fig. 8, with increasing the density the resistivity gradually approaches the regime where $\rho_{xx} \sim \sigma_{xx}$.

For critical temperatures $T_c \lesssim 0.2v_F\sqrt{|eB|}/c$ (i.e., for dependencies represented by thin solid and dashed lines), these two regimes correspond to two essentially different metal-insulator phase transitions. In the case of a small density (see the upper panel in Fig. 8), it is a conventional phase transition with insulator type and metallic type behaviors at temperatures below and just above T_c , respectively. On the other hand, for a large density (see the lower panel in Fig. 8), the “inverse” metal-insulator phase transition (with metal type dependence just below T_c and insulator type just above T_c) is realized.

Therefore we conclude that, in the presence of a magnetic field, a dynamical gap in the quasiparticle spectrum can indeed lead to a change of the insulator type dependence of $\rho_{xx}(T)$ to the metallic one. However, the nonzero Hall conductivity at finite density n complicates the picture and can lead to different types of metal-insulator phase transitions for small and large values of the charge density.

When the metal-insulator phase transition is truly a mean-field one, its clear signature is a kink in the resistivity $\rho_{xx}(T)$ at the critical point $T = T_c$. As has been already pointed out in the previous subsections, the $1/N_f$ fluctuations can change this feature, leading either to a discontinuity in the resistivity at $T = T_c$ (a first order phase transition) or to a smooth function $\rho_{xx}(T)$ (a higher order continuous phase transition).

VI. METAL-INSULATOR PHASE TRANSITION IN HIGHLY ORIENTED PYROLYTIC GRAPHITE

The main motivation of this study was the experimental data reported in Refs. 18–20. It was observed that samples of highly oriented pyrolytic graphite in an external magnetic field show a qualitative change of their resistivity as a function of temperature, that was interpreted as a metal-insulator phase transition. The effect is clearly seen only for a magnetic field perpendicular to the basal plane, suggesting that the orbital motion of quasiparticles is responsible for the change of the conductivity dependence.

In this section we will attempt to explain qualitatively the main features of the above mentioned experimental data in the light of the magnetic catalysis idea. We should note that the first step in this direction was made in Ref. 7. Here we go into further details utilizing the rather complete description of the magnetic catalysis in planar systems and its effect on the temperature depen-

dence of their conductivity and resistivity given in the previous sections.

First of all, the analysis made in Sec. V shows that, in the presence of a magnetic field, the flavor phase transition in planar systems can indeed manifest itself as a metal-insulator phase transition in the behavior of their resistivity $\rho(T)$ as a function of temperature. A noticeable fact is the existence of clearly distinguishable signatures of different types of the phase transition: the presence of a discontinuity and a kink in the resistivity $\rho(T)$ at the critical point $T = T_c$ in the cases of first order and mean field phase transitions, respectively, and a smooth behavior of $\rho(T)$ at $T = T_c$ for a continuous higher order phase transition. To the best of our knowledge, so far there have been no experiments reporting observations of a singular behavior of $\rho(T)$ at the critical point. At this stage, however, it would be premature to conclude that the observed phase transition is a continuous higher order one. This point deserves further experimental study.

A very interesting experimental observation made in Refs. 18–20 (and, to the best of our knowledge, has not been explained) is the existence of a finite “offset” magnetic field B_c . The value B_c determines the threshold $B = B_c$ for a qualitative change of the resistivity at zero temperature. More precisely, based on the experimental data, it was revealed²⁰ that the approximate relation for the critical temperature as a function of B reads $T_c(B) \sim \sqrt{B - B_c}$. This relation implies that at zero temperature the phase transition happens only when the magnetic field exceeds the threshold value $B = B_c$.

It is remarkable that, as was emphasized in Sec. IV, the existence of such a threshold B_c is a robust consequence of the mechanism of the magnetic catalysis. As was pointed out there, the value B_c is directly related to a nonzero charge density n of carriers,

$$|eB_c| = \frac{2\pi cn}{N_f}, \quad (101)$$

and this relation is exact. For example, by taking $B_c = 2.6 \times 10^4$ G, which was obtained in one of the experiments as an (upper) estimate of a critical value above which the generation of a gap presumably occurred,¹⁸ we derive the corresponding charge density (we use $N_f = 2$)

$$n = \frac{|eB_c|}{\pi c} = 1.25 \times 10^{-5} \text{ \AA}^{-2}. \quad (102)$$

This should be compared with the charge density (per unit area of a layer) of carriers in the used sample of graphite. By noting that the area per carbon atom in a layer is $S = \sqrt{3}a^2/4$ where the lattice spacing is $a \approx 2.46 \text{ \AA}$,¹¹ we conclude that the density in Eq. (102) corresponds to $n \approx 5 \times 10^{-6}$ units of charge per atom. While we do not know the exact density of the sample used, the given estimate is not unlikely.³²

Notice that the relation $T_c(B) \sim \sqrt{B - B_c} \equiv \sqrt{1 - \nu_B} \sqrt{B}$, used in Ref. 20, qualitatively differs from

our Eq. (72). It is quite remarkable, however, that the dependence $T_c(B)$ in Eq. (72) is nearly the same numerically as the simple square root relation suggested by the experimental data, see Fig. 9.

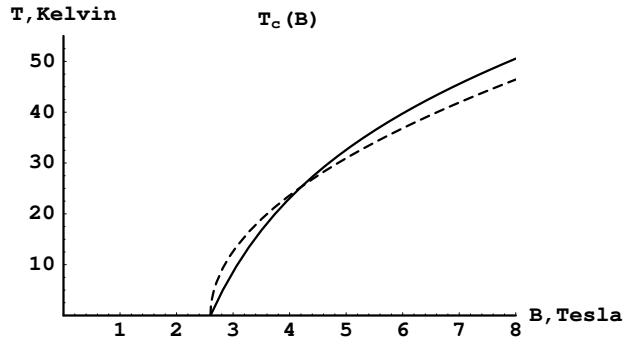


FIG. 9. The critical temperature as a function of a magnetic field. The solid line gives the dependence in Eq. (72), while the dashed line corresponds to a dependence with a simple field offset, i.e., $T_c \sim \sqrt{B - B_c}$. To plot the figure we used the following parameters: $N_f = 2$, $c/v_F = 375$, $\varepsilon_0 = 2.4$ and $B_c = 2.6 \times 10^4$ G.

Since the relation $|eB_c| = 2\pi cn/N_f$ is exact in the dynamics of the magnetic catalysis, its experimental verification would be a critical check of the validity of the scenario of the magnetic catalysis in highly oriented pyrolytic graphite.

Another noticeable experimental observation is that the scale of the critical temperature is set by the energy distance between the Landau levels (the Landau scale).^{18–20} Therefore, if the underlying physics of the transition is related to a dynamical generation of a gap, the typical values of the gap should also be of the same order as the Landau scale. As we discussed at length in Sec. IV, for the mechanism of the the magnetic catalysis this fact implies that the pairing dynamics corresponds to the strong coupling regime. This in turn implies that all (or many) Landau levels determine the pairing dynamics in this case. In connection with that, we would like to point out that, as the numerical analysis done in Sec. V shows, the contribution of higher Landau levels into the conductivity and resistivity become indeed important for values of the critical temperature T_c of the order of the Landau scale.

There still remain some unresolved issues in the interpretation of the experimental data in highly oriented pyrolytic graphite in a magnetic field.^{18–20} The most important of them is the observation of weak ferromagnetism in that system (for some speculations concerning its origin see Ref. 7). We hope to consider this issue elsewhere.

VII. CONCLUSION

In this paper we developed a theory of the magnetic field driven metal-insulator phase transition in planar systems, based on reduced QED. The general structure of the phase diagram of such systems was established in two cases, with and without an external magnetic field. The behavior of the electric conductivity (resistivity) in these systems was described in detail. This allowed us to conclude that, in the presence of a magnetic field, the flavor phase transition in planar systems can indeed manifest itself as a metal-insulator phase transition in the behavior of the resistivity $\rho(T, B)$ as a function of the magnetic field and temperature. It was also shown that there exist clearly distinguishable signatures of different types of the phase transition. While the resistivity $\rho(T)$ is a smooth function at the critical point $T = T_c$ in the case of a higher order continuous phase transition, there are a discontinuity and a kink in $\rho(T)$ at $T = T_c$ in the cases of the first order and mean field phase transitions, respectively.

Based on the experimental data,^{18–20} it has been recently argued that highly oriented pyrolytic graphite shows up a metal-insulator phase transition, driven by an external magnetic field.⁷ This might be a nonrelativistic realization of the phenomenon of the magnetic catalysis originally established in Refs. 13,14 in relativistic systems. In this paper we studied this possibility rather in detail, elaborating the theory of the magnetic catalysis in nonrelativistic planar systems and analyzing the temperature behavior of the resistivity (conductivity) in these systems. The conclusion of the present analysis concerning the possibility of this scenario in highly oriented pyrolytic graphite is quite positive.

One of the central results of this paper is establishing the *exact* relation (101) for the critical (threshold) value of the magnetic field at zero temperature in these systems. An experimental verification of this result would be a crucial test for the present theory.

Another conclusion of our investigation is that a nonzero magnetic field alone (even without producing a dynamical gap) can drastically change the general behavior of the resistivity as a function of temperature. In particular, in our simplest model with a constant value of the width parameter, the semiconductor type dependence of the resistivity [i.e., $\rho(T)$ decreasing with increasing temperature], seen in the absence of a magnetic field, can be replaced by a metallic type behavior [i.e., $\rho(T)$ increasing with temperature] in the region of not too high temperatures, when a nonzero field is turned on. In fact, at zero charge density of carriers, this change of behavior always happens in the range of temperatures $0 < T \lesssim 0.2v_F\sqrt{|eB|}/c$. This is also seen at finite but small densities when the diagonal component of conductivity dominates over the Hall conductivity.

We expect that the results of this paper will be useful for a wide class of condensed matter planar systems.

ACKNOWLEDGMENTS

We would like to thank D. Khveshchenko for numerous valuable discussions and bringing Ref. 30 to our attention. I.A.S. would like to thank B. Shklovskii for useful discussions. The research of V.P.G. has been supported in part by the National Science Foundation under Grant No. PHY-0070986 and by the SCOPES-projects 7 IP 062607 and 7UKPJ062150.00/1 of Swiss NSF. The work of I.A.S. was supported by the U.S. Department of Energy Grant No. DE-FG02-87ER40328.

APPENDIX A: SYMMETRY OF 2 + 1 DIMENSIONAL FERMIONS

In this Appendix we will consider the symmetry of 4-component fermions on a 2-brane which carry the flavor index $i = 1, 2, \dots, N_f$. The three 4×4 γ -matrices in Eq. (5) can be taken to be

$$\gamma^0 = \begin{pmatrix} \sigma_3 & 0 \\ 0 & -\sigma_3 \end{pmatrix}, \quad (\text{A1})$$

$$\gamma^1 = \begin{pmatrix} i\sigma_1 & 0 \\ 0 & -i\sigma_1 \end{pmatrix}, \quad (\text{A2})$$

$$\gamma^2 = \begin{pmatrix} i\sigma_2 & 0 \\ 0 & -i\sigma_2 \end{pmatrix}. \quad (\text{A3})$$

Recall that in 2 + 1 dimensions, two sets of matrices $(\sigma_3, i\sigma_1, i\sigma_2)$ and $(-\sigma_3, -i\sigma_1, -i\sigma_2)$ make inequivalent representations of the Clifford (Dirac) algebra

$$\gamma^\mu \gamma^\nu + \gamma^\nu \gamma^\mu = 2g^{\mu\nu}, \quad (\text{A4})$$

where $\mu, \nu = 0, 1, 2$ and $g^{\mu\nu} = \text{diag}(1, -1, -1)$.

There are two matrices,

$$\gamma^3 = i \begin{pmatrix} 0 & 1 \\ 1 & 0 \end{pmatrix}, \quad \gamma^5 = i \begin{pmatrix} 0 & 1 \\ -1 & 0 \end{pmatrix}, \quad (\text{A5})$$

that anticommute with γ^0, γ^1 and γ^2 . Therefore for each four-component spinor, there is a global $U(2)$ symmetry with the generators

$$I, \quad \frac{1}{i}\gamma^3, \quad \gamma^5, \quad \text{and} \quad \frac{1}{2}[\gamma^3, \gamma^5]. \quad (\text{A6})$$

Since there are N_f fermion flavors, the full symmetry of the action (10) is $U(2N_f)$ with the generators

$$\frac{\lambda^\alpha}{2}, \quad \frac{\lambda^\alpha}{2i}\gamma^3, \quad \frac{\lambda^\alpha}{2}\gamma^5, \quad \text{and} \quad \frac{\lambda^\alpha}{2} \frac{1}{2}[\gamma^3, \gamma^5], \quad (\text{A7})$$

where $\lambda^\alpha/2$, with $\alpha = 0, 1, \dots, N_f^2 - 1$, are N_f^2 generators of $U(N_f)$.

Adding a mass (gap) term $\Delta_0 \bar{\psi} \psi$ into the action (10) would reduce the $U(2N_f)$ symmetry down to the $U(N_f) \times U(N_f)$ with the generators

$$\frac{\lambda^\alpha}{2}, \quad \frac{\lambda^\alpha}{2} \frac{1}{2} [\gamma^3, \gamma^5], \quad (\text{A8})$$

with $\alpha = 0, 1, \dots, N_f^2 - 1$. This implies that the dynamical generation of the fermion gap leads to the spontaneous breakdown of the $U(2N_f)$ down to the $U(N_f) \times U(N_f)$.

APPENDIX B: DERIVATION OF POLARIZATION FUNCTION AND GAP EQUATION

In this Appendix, we give the details of the calculations of the time component of the gauge field polarization function, as well as the derivation of the gap equation at finite chemical potential and finite temperature. We will consider only the case of zero magnetic field. The polarization function and the gap equation in 2+1 dimensional QED with an external magnetic field was given in Ref. 28 where the method of Ref. 14 was used.

1. Polarization function

The general expression of the time component of the vacuum polarization function is given by²⁹

$$\begin{aligned} \Pi(\Omega_m, \vec{p}) &= \frac{2\pi}{\varepsilon_0} e^2 T N_f \sum_{n=-\infty}^{+\infty} \int \frac{d^2 k}{(2\pi)^2} \\ &\times \text{tr} \left[\gamma_0 S(\Omega_m + \omega_n, \vec{p} + \vec{k}) \gamma_0 S(\omega_n, \vec{k}) \right], \quad (\text{B1}) \end{aligned}$$

where $S(\omega_n, \vec{k})$ is the fermionic quasiparticle propagator whose explicit form reads

$$S(\omega_n, \vec{k}) = \frac{i}{(i\omega_n - \mu)\gamma_0 + (\vec{k} \cdot \vec{\gamma}) + \Delta_T(\mu)}. \quad (\text{B2})$$

In Eq. (B1), the Matsubara frequencies are denoted by $\omega_n \equiv (2n+1)\pi T$ and $\Omega_m \equiv 2m\pi T$. Also notice that the expression on the right hand side is multiplied by an additional factor $2\pi/\varepsilon_0$, in accordance with our definition of the polarization function. After taking the trace over the Dirac indices and using the Feynman parametrization, we obtain

$$\begin{aligned} \Pi(0, \vec{p}) &= \frac{8\pi}{\varepsilon_0} e^2 T N_f \sum_{n=-\infty}^{+\infty} \int_0^1 dx \int \frac{d^2 k}{(2\pi)^2} \\ &\times \left[\frac{1}{(\omega_n + i\mu)^2 + v_F^2 p^2 x(1-x) + v_F^2 k^2 + \Delta_T^2(\mu)} \right. \\ &\left. - \frac{2[v_F^2 k^2 + \Delta_T^2(\mu)]}{[(\omega_n + i\mu)^2 + v_F^2 p^2 x(1-x) + v_F^2 k^2 + \Delta_T^2(\mu)]^2} \right]. \quad (\text{B3}) \end{aligned}$$

By calculating the sum over n , we get

$$\begin{aligned} \Pi(0, \vec{p}) &= \frac{e^2 N_f}{2\varepsilon_0} \int_0^1 dx \int_0^\infty \frac{dk^2}{Y^2} \left[\frac{v_F^2 p^2 x(1-x)}{Y} \right. \\ &\left. \times \tanh \frac{Y + \mu}{2T} + \frac{v_F^2 k^2 + \Delta_T^2(\mu)}{2T \cosh^2 \frac{Y + \mu}{2T}} + (\mu \rightarrow -\mu) \right], \quad (\text{B4}) \end{aligned}$$

where $Y = \sqrt{v_F^2 k^2 + v_F^2 p^2 x(1-x) + \Delta_T^2(\mu)}$. By changing the integration variable, $k^2 \rightarrow Y$, and integrating by parts, we finally arrive at the following convenient representation:

$$\begin{aligned} \Pi(0, \vec{p}) &= \frac{2T e^2 N_f}{\varepsilon_0 v_F^2} \int_0^1 dx \left[\ln \left(2 \cosh \frac{R_x + \mu}{2T} \right) \right. \\ &\left. - \frac{\Delta_T^2(\mu)}{2T R_x} \tanh \frac{R_x + \mu}{2T} + (\mu \rightarrow -\mu) \right], \quad (\text{B5}) \end{aligned}$$

where $R_x = \sqrt{v_F^2 p^2 x(1-x) + \Delta_T^2(\mu)}$.

2. Gap equation

The general Schwinger-Dyson equation for the quasi-particle propagator reads

$$\begin{aligned} S^{-1}(\omega_m, \vec{p}) &= S_0^{-1}(\omega_m, \vec{p}) - T \sum_{n=-\infty}^{\infty} \int \frac{d^2 k}{(2\pi)^2} \\ &\times \gamma^0 S(\omega_n, \vec{k}) \gamma^0 U(\vec{p} - \vec{k}). \quad (\text{B6}) \end{aligned}$$

By neglecting the wave function renormalization,²⁴ we derive the following gap equation:

$$\begin{aligned} \Delta(p) &= \frac{e^2 T}{2\pi\varepsilon_0} \sum_{n=-\infty}^{+\infty} \int \frac{\Delta(k) d^2 k}{(\omega_n + i\mu)^2 + v_F^2 k^2 + \Delta_T^2(\mu)} \\ &\times \frac{1}{|\vec{p} - \vec{k}| + \Pi(0, \vec{p} - \vec{k})}. \quad (\text{B7}) \end{aligned}$$

Here the interaction is taken in the so-called instantaneous exchange approximation. This means that the retardation effects of the gauge field are neglected which is justified in a nonrelativistic model.

By neglecting the dependence of the gap on the Matsubara frequency, we could perform the sum over n explicitly. Then, the result reads

$$\begin{aligned} \Delta(p) &= \frac{\pi e^2}{\varepsilon_0} \int \frac{d^2 k}{(2\pi)^2} \frac{\Delta(k)}{E_k} \frac{\sinh \frac{E_k}{T}}{\cosh \frac{E_k}{T} + \cosh \frac{\mu}{T}} \\ &\times \frac{1}{|\vec{p} - \vec{k}| + \Pi(0, \vec{p} - \vec{k})}, \quad (\text{B8}) \end{aligned}$$

where $E_k = \sqrt{v_F^2 k^2 + \Delta_T^2(\mu)}$. By using the standard approximation for the kernel of the integral equation, $f(|\vec{p} - \vec{k}|) \rightarrow f(p)\theta(p-k) + f(k)\theta(k-p)$, we obtain the following gap equation:

$$\Delta(p) = \frac{e^2}{2\varepsilon_0 v_F} \int_{\epsilon}^{\Lambda} dk \Delta(k) \frac{\sinh \frac{v_F k}{T}}{\cosh \frac{v_F k}{T} + \cosh \frac{\mu}{T}} \times \left[\frac{\theta(p-k)}{p + \Pi(0, \vec{p})} + \frac{\theta(k-p)}{k + \Pi(0, \vec{k})} \right], \quad (\text{B9})$$

where the infrared cutoff ϵ is given by a larger value of $\Delta_T(\mu)/v_F$ or $\sqrt{\mu^2 - \Delta_T^2(\mu)}/v_F$, and where we also utilized the bifurcation method in which a nonlinear gap equation is replaced by a linear approximation (compare with the discussion in subsection III B). This is achieved by substituting the trivial value of the gap in E_k and introducing an infrared cutoff in the integral on the right hand side of Eq. (B8).

APPENDIX C: DERIVATION OF EFFECTIVE POTENTIAL AT $\mu \neq 0$

In this appendix, we will construct the effective potential of the composite field $\sigma = -\langle \bar{\psi} \psi \rangle$ by using the method of Ref. 33. For the purposes of this paper, it is sufficient to consider only the case of a nonzero chemical potential. The generalization to some other cases (for example, with an external magnetic field) is also possible, see for example Ref. 34.

In order to derive the effective potential as a function of the composite field σ , one should introduce a term with a constant external source J coupled to the corresponding composite operator in the action, and construct the generating functional $W(J)$. The effective potential, then, is defined through the Legendre transform as follows:³³

$$V(\sigma) = -w(J) + J\sigma = \int^{\sigma} d\sigma J(\sigma), \quad (\text{C1})$$

where $w(J) \equiv W(J)/V_{2+1}$, and V_{2+1} is the space-time volume of a 2-brane. In the last expression, the source J should be regarded as a function of the field σ .

The effect of the external source J could be easily taken into account in the gap equation (29): one should simply replace $\Delta_p \rightarrow \Delta_p - J$ on the left hand side of the equation. Then, the solution to the equation, satisfying the infrared boundary condition, takes the following form:

$$\Delta_p = \frac{\Delta}{\sin \delta} \sqrt{\frac{\epsilon}{p}} \sin \left[\frac{\nu}{2} \ln \frac{p}{\epsilon} + \delta \right], \quad (\text{C2})$$

where $\nu = \sqrt{4\lambda - 1}$, $\epsilon = \max\{\Delta/v_F, \sqrt{\mu^2 - \Delta^2}/v_F\}$, and $\delta = \arctan \nu$. The overall normalization of the above solution is fixed by choosing $\Delta_{p=\epsilon} = \Delta$. The ultraviolet boundary condition,

$$J = (\Delta_p + p\Delta'_p)|_{p=\Lambda}, \quad (\text{C3})$$

on the other hand, produces the relation:

$$J = \frac{\Delta}{\sin(2\delta)} \sqrt{\frac{\epsilon}{\Lambda}} \sin \left[\frac{\nu}{2} \ln \frac{\Lambda}{\epsilon} + 2\delta \right]. \quad (\text{C4})$$

As it should be, the equation for the dynamical gap Δ_0 is obtained in the limit of vanishing source $J = 0$. At zero chemical potential, in particular, the equation for the gap takes the form:

$$\frac{\nu}{2} \ln \frac{\Lambda v_F}{\Delta_0} = \pi - 2\delta. \quad (\text{C5})$$

For the derivation of the effective potential, we also need to know the expression for the field σ . By definition, it is equal to the trace of the fermion propagator. Thus, we get

$$\sigma = -\langle \bar{\psi} \psi \rangle = -\frac{N_f}{\pi \lambda v_F} p^2 \Delta'(p) \Big|_{p=\Lambda} = \frac{N_f \Delta \sqrt{\epsilon \Lambda}}{\pi \lambda v_F \sin(2\delta)} \sin \left[\frac{\nu}{2} \ln \frac{\Lambda}{\epsilon} \right]. \quad (\text{C6})$$

Now, by making use of Eq. (C5), we trade the cutoff parameter Λ for Δ_0 . After that, we derive the following approximate relations for the case of small ν we are interested in:

$$J(\Delta) \simeq -\frac{\Delta}{4} \sqrt{\frac{\epsilon}{\Lambda}} \ln \frac{\Delta_0}{\epsilon v_F}, \quad (\text{C7})$$

$$\sigma(\Delta) \simeq \frac{N_f \Delta \sqrt{\epsilon \Lambda}}{\pi v_F} \left(4 - \ln \frac{\Delta_0}{\epsilon v_F} \right). \quad (\text{C8})$$

As will become clear in a moment, these two expressions contain all the information needed for reconstructing the potential. Indeed, the definition of the effective potential in Eq. (C1) can be rewritten as follows:

$$V(\sigma) = \int^{\Delta} d\Delta \frac{d\sigma(\Delta)}{d\Delta} J(\Delta) + f(\mu), \quad (\text{C9})$$

where the most general integration constant $f(\mu)$ was added on the right hand side. This new representation leads to the final result,

$$V(\Delta) = \frac{N_f \Delta^2 \sqrt{\mu^2 - \Delta^2}}{2\pi v_F^2} \left[\frac{1}{4} \ln^2 \frac{\sqrt{\mu^2 - \Delta^2}}{\Delta_0} + \ln \frac{\sqrt{\mu^2 - \Delta^2}}{\Delta_0} - \frac{2\mu^2 + \Delta^2}{3\Delta^2} \right] + f_1(\mu), \quad (\text{C10})$$

for $\Delta \leq |\mu|/\sqrt{2}$, and

$$V(\Delta) = \frac{N_f \Delta^3}{2\pi v_F^2} \left[\frac{1}{4} \ln^2 \frac{\Delta}{\Delta_0} + \ln \frac{\Delta}{\Delta_0} - \frac{1}{3} \right] + f_2(\mu), \quad (\text{C11})$$

for $\Delta \geq |\mu|/\sqrt{2}$. In these equations we used the freedom of choosing the integration constants in expressions (C10) and (C11) as follows:

$$f_1(\mu) = \frac{\sqrt{2} N_f |\mu|^3}{6\pi v_F^2} + f_2(\mu), \quad (\text{C12})$$

$$f_2(\mu) = -\frac{N_f(|\mu| - \Delta_0)^2(|\mu| + 2\Delta_0)}{6\pi v_F^2} \\ \times \theta(|\mu| - \Delta_0)\theta(\mu_c - |\mu|) \\ - \frac{N_f[|\mu|^3 - \Delta_0^2(3\mu_c - 2\Delta_0)]}{6\pi v_F^2}\theta(|\mu| - \mu_c). \quad (\text{C13})$$

This choice insures that the potential is continuous at the matching point $\Delta = |\mu|/\sqrt{2}$, and that it is normalized so that its partial derivative with respect to the chemical potential at the global minimum is equal (up to a sign) to the charge density:

$$\frac{\partial V(\Delta_0, \mu)}{\partial \mu} \equiv \frac{N_f(\Delta_0^2 - \mu^2)}{2\pi v_F^2} \text{sgn}(\mu)\theta(|\mu| - \Delta_0), \quad (\text{C14})$$

for $|\mu| < \mu_c$, and

$$\frac{\partial V(0, \mu)}{\partial \mu} \equiv -\frac{N_f\mu^2}{2\pi v_F^2} \text{sgn}(\mu), \quad (\text{C15})$$

for $|\mu| > \mu_c$. Here we used the expression for the charge density in Eq. (85).

Now, the effective potential as a function of the composite field σ is defined parametrically through Eqs. (C10), (C11) and (C8). This dependence is graphically shown in Fig. 2 for a few different values of the chemical potential. As is clear from the figure, the presence of a nonzero chemical potential considerably changes the behavior of the effective potential. In particular, a new local minimum develops at the origin and its depth gradually increases with μ . The competition of the two minima, located at $\sigma = 0$ and $\sigma_0 \equiv \sigma(\Delta_0)$, results in a first order phase transition. Such a transition happens when the depths of effective potential at its two minima become equal. By making use of this criterion, we derive the analytical expression for the critical value of the chemical potential,

$$\mu_c = \frac{\Delta_0}{(2 - \sqrt{2})^{1/3}} \simeq 1.195\Delta_0. \quad (\text{C16})$$

Note that this result is valid in the limit of vanishing ν . At small ν , the critical value gets an additional correction of order ν^4 . The numerical analysis shows that the explicit form of such a correction is about $-0.044\nu^4\Delta_0$.

* On leave of absence from Bogolyubov Institute for Theoretical Physics, 252143, Kiev, Ukraine.

¹ E. Fradkin, *Field Theories of Condensed Matter Systems* (Addison-Wesley, Redwood City, CA, 1991).

² J. B. Marston and I. Affleck, Phys. Rev. B **39**, 11538 (1989); J. B. Marston, Phys. Rev. Lett. **64**, 1166 (1990); A. Kovner and B. Rosenstein, Phys. Rev. B **42**, 4748 (1990);

N. Dorey and N. E. Mavromatos, Nucl. Phys. B **386**, 614 (1992); I. J. R. Aitchison and N. E. Mavromatos, Phys. Rev. B **53**, 9321 (1996).

³ M. Franz and Z. Tešanović, Phys. Rev. Lett. **84**, 554 (2000); L. Marinelli, B. I. Halpern, and S. H. Simon, Phys. Rev. B **62**, 3488 (2000); O. Vafek, A. Melikyan, M. Franz, and Z. Tešanović, Phys. Rev. B **63**, 134509 (2001); J. Ye, Phys. Rev. Lett. **86**, 316 (2001); A. Vishwanath, Phys. Rev. Lett. **87**, 217004 (2001).

⁴ K. Farakos, G. Koutsoumbas and N. E. Mavromatos, Int. J. Mod. Phys. B **12**, 2475 (1998); G. W. Semenoff, I. A. Shovkovy and L. C. R. Wijewardhana, Mod. Phys. Lett. A **13**, 1143 (1998); W. V. Liu, Nucl. Phys. B **556**, 563 (1999); E. J. Ferrer, V. P. Gusynin and V. de la Incera, arXiv:hep-ph/0101308.

⁵ G. W. Semenoff, Phys. Rev. Lett. **53**, 2449 (1984).

⁶ J. González, F. Guinea, and M. A. H. Vozmediano, Phys. Rev. B **59**, R2474 (1999); Phys. Rev. B **63**, 134421 (2001).

⁷ D. V. Khveshchenko, Phys. Rev. Lett. **87**, 206401 (2001).

⁸ D. V. Khveshchenko, Phys. Rev. Lett. **87**, 246802 (2001).

⁹ E. V. Gorbar, V. P. Gusynin and V. A. Miransky, Phys. Rev. D **64**, 105028 (2001).

¹⁰ J. Alexandre, K. Farakos, G. Koutsoumbas and N. E. Mavromatos, Phys. Rev. D **64**, 125007 (2001).

¹¹ P. R. Wallace, Phys. Rev. **71**, 622 (1947).

¹² J. W. McClure, Phys. Rev. **108**, 612 (1957).

¹³ V. P. Gusynin, V. A. Miransky, and I. A. Shovkovy, Phys. Rev. Lett. **73**, 3499 (1994); Phys. Rev. D **52**, 4718 (1995);

¹⁴ V. P. Gusynin, V. A. Miransky, and I. A. Shovkovy, Phys. Rev. D **52**, 4747 (1995). Nucl. Phys. B **462**, 249 (1996).

¹⁵ S. Kawati, G. Konisi and H. Miyata, Phys. Rev. D **28**, 1537 (1983); S. P. Klevansky and R. H. Lemmer, Phys. Rev. D **39**, 3478 (1989); H. Suganuma and T. Tatum, Annals Phys. **208**, 470 (1991).

¹⁶ K. G. Klimenko, Z. Phys. C **54**, 323 (1992); I. V. Krive and S. A. Naftulin, Phys. Rev. D **46**, 2737 (1992).

¹⁷ V. A. Miransky, Prog. Theor. Phys. Suppl. **123**, 49 (1996); Y. J. Ng, arXiv:hep-th/9803074; C. N. Leung, arXiv:hep-th/9806208; V. P. Gusynin, Ukr. J. Phys. **45**, 603 (2000).

¹⁸ Y. Kopelevich, et al., Phys. Solid State **41**, 1959 (1999).

¹⁹ H. Kempa, et al., Solid State Comm. **115**, 539 (2000).

²⁰ S. M. Sercheli, et al., arXiv:cond-mat/0106232.

²¹ R. Jackiw and S. Templeton, Phys. Rev. D **23**, 2291 (1981); S. Deser, R. Jackiw and S. Templeton, Ann. Phys. (N. Y.) **140**, 372 (1982).

²² R. D. Pisarski, Phys. Rev. D **29**, 2423 (1984); T. W. Appelquist, M. Bowick, D. Karabali and L. C. Wijewardhana, Phys. Rev. D **33**, 3704 (1986); *ibid.* D **33**, 3774 (1986).

²³ The symmetry $U(2N_f)$ can be also explicitly broken by additional local interactions (e.g., four-fermion ones) possessing a lower symmetry.

²⁴ The wave function renormalization is a next to the leading order effect in the $1/N_f$ expansion. The experience of working with the gap equation in QED₂₊₁ suggests that neglecting it does not affect results too much even for values of N_f of order one. For example, in the Landau gauge, the critical value for the number of fermion flavors is $N_f^{cr} \simeq 3.24$ and $N_f^{cr} \simeq 4.32$ in the cases of neglecting the wave function renormalization and taking it into account, respectively.²⁶

²⁵ T. Appelquist, D. Nash and L. C. Wijewardhana, Phys.

- Rev. Lett. **60**, 2575 (1988).
- ²⁶ D. Nash, Phys. Rev. Lett. **62**, 3024 (1989). K.-I. Kondo and H. Nakatani, Mod. Phys. Lett. A **5**, 407 (1990); P. Maris, Phys. Rev. D **52**, 6087 (1995); V. P. Gusynin, A.H. Hams, and M. Reenders, Phys. Rev. D **53**, 2227 (1996); *ibid* **63**, 045025 (2001). I.J. Aitchison, N.E. Mavromatos, and D. McNeill, Phys. Lett. B **402**, 154 (1997);
- ²⁷ V. P. Gusynin, V. A. Miransky and I. A. Shovkovy, Phys. Rev. Lett. **83**, 1291 (1999); Nucl. Phys. B **563**, 361 (1999).
- ²⁸ A. V. Shpagin, arXiv:hep-ph/9611412.
- ²⁹ We use the symbols G and S for the fermion propagator in the cases with and without magnetic field, respectively.
- ³⁰ A. C. Durst and P. A. Lee, Phys. Rev. B **62**, 1270 (2000).
- ³¹ E. J. Ferrer, V. P. Gusynin and V. de la Incera, arXiv:cond-mat/0203217.
- ³² B. T. Kelly, *Physics of Graphite*, (Applied Science Publishers, London; Englewood, N.J., 1981).
- ³³ V. A. Miransky, Int. J. Mod. Phys. **A 8**, 135 (1993).
- ³⁴ D. S. Lee, P. N. McGraw, Y. J. Ng, and I. A. Shovkovy, Phys. Rev. D **59**, 085008 (1999).